Département de géomatique appliquée
Faculté des lettres et sciences humaines

Université de Sherbrooke

Analyse de l'effet des lacs sur le bilan d'énergie de surface régionale dans le nord du Canada avec l'apport d'images satellites

Use of satellite data to estimate regional surface energy budget and analysis of lake cover impact over Northern Canada

Vahid Ikani

Mémoire présenté pour l'obtention du grade de Maître ès sciences géographiques

(M.Sc.), cheminement Télédétection

May 2009

Composition du jury

Analyse de l'effet des lacs sur le bilan d'énergie de surface régionale dans le nord du Canada avec l'apport d'images satellites

Use of satellite data to estimate regional surface energy budget and analysis of lake cover impact over Northern Canada

Vahid Ikani

Ce mémoire a été évalué par un jury composé des personnes suivantes :

Directeur de recherche : Alain Royer
Université de Sherbrooke
Département de Géomatique Appliquée, Faculté des lettres et sciences humaines

Lecteur externe : Laxima Sushama
Université du Québec à Montréal (UQAM)
Département des Sciences de la Terre et de l'Atmosphère, Faculté des sciences

Lecteur interne : Hardy B. Granberg
Université de Sherbrooke
Département de Géomatique Appliquée, Faculté des lettres et sciences humaines

Résumé

Les lacs occupent environ 30% du territoire dans le nord du Canada. Ils peuvent avoir d'importants impacts sur le climat qui ont un effet par la suite sur les propriétés thermiques des lacs. L'étude d'un lac doit généralement débuter avec un bilan calorifique de la surface. La différentiation précise que l'énergie disponible en flux de chaleur sensible ou latent est un élément crucial pour la compréhension des interactions entre les processus climatiques à une échelle régionale.

Dans cette étude, le flux de chaleur sensible et le ratio de Bowen sont obtenus à partir des données de la télédétection. La méthodologie se base sur l'utilisation de données micro-ondes (SMM/I) afin de calculer la température de la surface du sol avec la méthode de Fily et al. (2003) et Mialon et al. (2007). La caractérisation de la surface du sol est effectuée à partir de données satellitaires optiques (capteurs SPOT & VGT). Les paramètres météorologiques utilisés pour estimer les flux proviennent de la base de données du North American Regional Reanalysis (NARR).

Les résultats présentent un portrait quotidien, mensuel et saisonnier de l'énergie sensible à l'interface sol-air par rapport à la fraction de la surface de plan d'eau (FWS). Nous comparons ensuite nos résultats avec les flux du modèle NARR et quelques mesures in situ.

Quatre sites couvrants différents types de surfaces à travers le Canada ont été étudiés pendant les étés 1998 et 2000 (de juin à septembre) : le nord du Québec (toundra), les Territoires du Nord-Ouest (le Grand lac des Esclaves [ou, en anglais, Great Slave Lake - GSL] et le bassin de la rivière Mackenzie), le Manitoba (zone humide) et le Labrador (taïga).

Les résultats montrent que les flux d'énergie sensible satellitaires sont semblables aux flux estimés par le NARR lorsque la FWS est petit (sans lac) ou pour des zones avec de larges surfaces d'eau (Mackenzie Great Slave Lake), mais diffèrent lorsque la FWS augmente à l'intérieur d'un pixel. Ceci signifie que les modèles climatiques régionaux devraient considérer la proposition du territoire occupée par des étendues d'eau. Nous déduisons que les effets de la taille des lacs sont reliés aux conditions environnementales du milieu. Les résultats de la comparaison avec des mesures in situ pour le GSL et la zone humide sont encourageants.

Le ratio de Bowen sur le site du bassin de la rivière Mackenzie montre qu'il y a une augmentation de la chaleur sensible durant la deuxième moitié de l'été en comparaison à la première moitié. Il y a ainsi un plus grand stress hydrique pendant la deuxième moitié de l'été. Cependant, il n'y a pas de patrons clairs en comparaison avec le site GSL. La comparaison entre les différents sites indique une variation énergétique annuelle minimale pour la zone humide.

Mots-clés : Modèle climatique régional, Micro-ondes passives (SSM/I), Flux de chaleur sensible, Ratio de Bowen, FWS, Température de surface normalisée, Résistance de bulk.

Abstract

Lakes occupy roughly 30% of Canada's northern landscape. They can have important impacts on the climate, and climate modification will affect lake thermal properties. Study of a lake most generally begins with heat budget at its surface. Accurate partitioning of the available energy at the surface into sensible and latent heat flux is crucial to the understanding of interactions between climate processes on a regional scale.

In this study, sensible heat flux and the Bowen ratio for the summer period are retrieved using reanalysis and remote sensing data. The methodology is based on the use of microwave data for retrieving land surface temperature (SSM/I) with the method of Fily et al. (2003) and Mialon et al. (2007). The land cover characterization is derived from remotely sensed optical data (SPOT VGT sensor). Some meteorological parameters used for retrieving flux are derived from the North American Regional Reanalysis (NARR) database.

The results from this study present a picture of the daily, monthly and seasonally sensible energy over summer period at the land-air interface versus the Fraction of Water Surface (FWS). We compare our results with the NARR model's flux in addition to few in situ measurements.

Four sites covering different land cover types across Canada were investigated during the 1998 and 2000 summers (June to September): Northern Quebec (tundra), Northwest Territories (Great Slave Lake, or GSL, and Mackenzie River Basin), Manitoba (wetlands) and Labrador (taiga).

The results show that the satellite-derived sensible flux is close to the NARR flux estimate when the fraction of water surface is small (no lakes) and over large open water areas (Mackenzie Great Slave Lake), but differs when the FWS increases within the pixel. This means that regional climate models should take into account lake cover fraction. We infer that effects of the lake-size are closely related to surrounding environmental conditions. The results of the comparison with in situ measurements for Great Slave Lake (1998) and the Wetland site are encouraging.

For the Mackenzie River Basin site, the results of the Bowen ratio show that there is an increase of sensible heat partition during the second half of the summer in comparison with the first half, meaning that there is more water stress over the second half of the summer than the first. But for the Wetland site, there is no clear pattern, and in comparison with GSL, temporal variation is less significant. Comparisons between different sites indicate minimum year to year energy variation for the Wetland area.

Keywords: Regional climate model, Passive microwave SSM/I, Sensible heat flux, Bowen ratio, Fraction of Water Surface, Normalized Surface Temperature, Bulk resistance.

Table of contents

Table of contents		v
List of figures		vii
List of tables		ix
List of Appendix		ix
Glossary		x
1.	Introduction	1
1.1	Problem	1
1.2.	Objectives	7
1.3.	Hypothesis	7
1.4.	Plan	8
2.	The energy budget constraint	8
3.	Site description	11
4.	Data description	12
5.	Methodology	14
5.1	Data processing	14
5.1.1	Temperature derived from satellite measurements	16
5.1.2	Determination of fractional water surface	16
5.1.3	Satellite-derived temperature daily normalization	17
5.1.4	Image processing	18
5.1.5	Extraction the NARR data	19
5.2	Retrieval of sensible heat flux from satellite data	20
5.2.1	Retrieved sensible heat flux	20
5.2.2	Estimation of latent heat and Bowen ratio	24
5.3	Temperature condition	25
6.	Results	25

6.1	Comparison between retrieved and modelled sensible heat flux	25
6.2	Importance of lake size	33
6.3	Seasonal (monthly) sensible heat fluxes variation	35
6.4	Site to site Comparison	41
6.5	Comparison between 1998 and 2000	47
6.6	Bowen ratio estimation – "GSL" and "wetland" sites	49
6.7	Comparisons with in situ measurements	50
7.	Conclusions and verification of hypothesis	57
8.	References	58

List of figures

1. Lake –wide average sensible and latent heat flux in 1999 (Great Slave Lake and Great Bear Lake) 4

2. Direction of sensible heat fluxes 9

3. Schematic figure of the heat budget of a thin interfacial layer near the surface (Source: Sun et al., 1995) 10

4. Location of the study sites 11

5. A quick view of the data and acquired sources 14

6. Algorithm used for study 15

7. Normalization process: applying ERA-40 diurnal cycle (dashed line) to satellite-derived temperature (x) derived from SSM/ I sensor leads to normalized (hourly) series (continuous) 18

8. Land cover classification of North American year 2000(Latifovic et al., 2002) (a) EASI-Grid projection and (b) visualization the same figure in geographical coordinates 19

9. Schematic description of models for heat transfer (source: Lia 2004) 21

10. The daily variation of sensible heat as a function of FWS for the GSL site - August 1998 26

11. The daily variation of sensible heat as a function of FWS for the GSL site - August 2000 27

12. The daily variation of sensible heat as a function of FWS for the GSL site - July 1998 28

13. The daily variation of sensible heat as a function of FWS for the GSL site - July 2000 29

14. Average sensible heat flux versus FWS%, GSL 31

15. Average sensible heat flux versus FWS%, Wetland 32

16. Daily values of sensible heat flux for GSL site for SL, ML and LL Classes separately, July and August 1998 34

17. Average surface-air temperature gradient versus FWS% for four months (July, August and September) of 1998 and 2000 for the GSL 37

18. Average sensible heat fluxes (retrieved) versus FWS% for four months (June, July, August and September) of 1998 and 2000 for the GSL 37

19. Average surface-air temperature gradient versus FWS% for four months (July, August and September) of 1998 and 2000 for the Tundra 38

20. Average sensible heat fluxes (retrieved) versus FWS% for four months (July, August and September) of 1998 and 2000 for the Tundra 38

21. Average surface-air temperature gradient versus FWS% for four months (June, July, August and September) of 1998 and 2000 for the Wetland 39

22. Average sensible heat fluxes (retrieved) versus FWS% for four months (June, July, August and September) of 1998 and 2000 for the Wetland 39

23. Average surface-air temperature gradient versus FWS% for four months (June, July, August and September) of 1998 and 2000 for the Taiga 40

24. Average sensible heat fluxes (retrieved) versus FWS% for four months (June, July, August and September) of 1998 and 2000 for the Taiga 40

25. Comparison between the 4 sites - modelled and retrieved values over the summers of 1998 42

26. Comparison between the 4 sites - modelled and retrieved values over the summers of 2000 43

27. Comparison between 4 sites, over 1998 and 2000, SF class 47

28. Comparison between 4 sites, over 1998 and 2000, MF class 48

29. Comparison between 4 sites, over 1998 and 2000, LF class 48

30. Bowen ratio as a function of FWS for the GSL – years 1998 and 2000 51

31. Bowen ratio as a function of FWS for the wetland – years 1998 and 2000 52

32. Spatial distribution of the H/R_{net} ratio for the "GSL", modelled and Retrieved 54

33. Spatial distribution of the H/R_{net} ratio for the "Wetland", modelled and Retrieved 56

List of tables

1. List of studies related to surface flux measurement derived from Jiang et al., 2004 6

2. The geographical coordinates of the study sites 12

3. Name of sites and close meteorological stations 25

4. Ratios (*y/x*) for GSL site 45

5. Ratios (*y/x)* for Wetland site 45

6. Ratios (*y/x*) for Tundra site 46

7. Ratios (*y/x*) for Taiga site 46

8. Bowen ratio values for the GSL site 50

9. Bowen ratio values for the wetland site 50

10. Comparison of H/R_{net} ratio with *in situ* (Rouse *et al.*, 2001) - GSL 53

11. Comparison of H/R_{net} ratio with *in situ* (Rouse *et al.*, 2001) - wetland 55

List of appendix

Appendix 1- Classification of land covers 66

Appendix 2- Values of aerodynamic roughness 67

Appendix 3- Temperature condition for the study sites 68

Appendix 4- The retrieved values for GSL site 69

Glossary

AVHRR	Advanced Very High Resolution Radiometer
CRCM	Canadian Regional Climate Model
C_p	Air specific heat at constant pressure ($\frac{J}{KgK}$)
d	Zero plane displacement (m)
DMSP	Defence Meteorological Satellite Program
E	Latent heat ($\frac{W}{m^2}$)
EASE Grid	Equal Area Scalable Equal Area
e_H	Emissivity at horizontal polarization
e_p	Emissivity at polarization p
e_v	Emissivity at vertical polarization
ew	Emissivity of water
FWS	Fraction of water surface
G	Ground heat flux ($\frac{W}{m^2}$)
G	Gravitational acceleration
GCM	General Circulation Model
GSL	Great Slave Lake

GRIB	GRIdded Binary
h_c	Canopy Height (m)
H	Sensible heat flux ($\frac{W}{m^2}$)
K	Kofeman Coefficient (Dimensionless)
kB^{-1}	Excess resistance parameter (Dimensionless)
L	Obukhov stability length (m)
L↓	Incoming long wave radiation ($\frac{W}{m^2}$)
L↑	Outgoing long wave radiation ($\frac{W}{m^2}$)
LF	Large Fraction of water surface
MAE	Mean Absolute Error
MF	Medium Fraction of water surface
MRB	Mackenzie River Basin
NF	No Fraction of water surface
NARR	North American Regional Reanalysis
NCEP	National Center for Environment Prediction
NSIDC	National Snow and Ice Data Center
POM	Princeton Ocean Model

R_{net}	Net radiation flux ($\frac{W}{m^2}$)
r_a	Aerodynamic resistance ($\frac{s}{m}$)
S↑	Outgoing short wave radiation ($\frac{W}{m^2}$)
S↓	Incoming shortwave radiation ($\frac{W}{m^2}$)
SF	Small Fraction of water surface
SSM/I	Special Sensor Microwave Image
T_a	Air temperature (K°)
T_{ab}	Downward atmospheric contribution
T_{au}	Upward atmospheric contribution
TBH	Apparent brightness temperature at horizontal polarization (satellite level)
TBV	Apparent brightness temperature at vertical polarization (satellite level)
TB_P	Apparent brightness temperature at satellite level
T_s	Surface temperature (K°)
U	Wind velocity in X direction ($\frac{m}{s}$)
V	Wind velocity in Y direction ($\frac{m}{s}$)
W	Wind speed ($\frac{m}{s}$)

Z_0	Reference height (m)	
Z	Reference height Aerodynamic roughness length (m)	
ψ_h	Stability correction function for heat transfer	(Dimensionless)
ψ_m	Stability correction function for momentum transfer	(Dimensionless)
β	Bowen ratio (H/ (R_{net} -H))	(Dimensionless)
ρ	Air density ($\frac{kg}{m^3}$)	

Remerciements

Je tiens à remercier en premier lieu le Professeur Alain Royer pour son soutien scientifique, ses avis, ses encouragements, sa patience et sa bonne humeur.

Je tiens aussi à exprimer ma reconnaissance au Conseil de Recherches en Sciences Naturelles et en Génie du Canada qui a permis de financé cette recherche.

Un grand merci à l'équipe DAI (Donnée Accès Intégration) pour les donnes de NARR, la Cartothèque de l'université de Sherbrooke et Stéphane Poirier de l'équipe de Royer et GEC3.

1. Introduction

An understanding of the energy budget of lakes and wetlands and their interaction with the atmosphere is crucial for assessing the impacts of resource development and climate change (Long et al., 2007). In recent years, various studies have been conducted to estimate surface energy fluxes using remote sensing techniques. Remotely sensed data are the only tools that have the potential to provide spatially distributed information relating to land surface parameters and state variables on a regular basis, on a range of spatial scales. This information is potentially very useful in hydrology and meteorology for quantifying the spatially distributed parameters and variables that control the interaction of land surface and atmospheric processes (Humes et al., 1997).

In this study we estimate sensible heat flux and its variations as a function of the Fraction of Water Surface (FWS). For the purpose of this study, based on method Fily et al (2003), Mialon (2005) and SSM/I data, an algorithm for estimating sensible heat flux was developed. The SSM/I data are applicable any time of day, in all weather conditions, and provide a resolution of 25 km. In the following section, the problem will be discussed. The objectives and hypotheses are then explained. Finally, we present the plan of the thesis.

1.1 Problem

Canada has nearly two million fresh water lakes ranging in size from less than 1 km^2 up to some of the largest lakes in the world. The lakes occupy roughly 30% of Canada's northern landscape. Because of their abundance, lakes are important factors pertaining to the regional climate. Air and water exchanges of heat and moisture have climatological implications not only on water bodies but also on the climate of the overlying air and the areas adjacent to water masses (Long et al., 2007).

Swayne et al. (2004) indicated that the inland water (lakes, wetlands) can have important impacts on the climate on various spatial scales; also, climate variations will affect lake

thermal properties. Furthermore, Nagarajan et al. (2004) conclude that small lakes have a substantial effect on the atmospheric heat and water budgets.

On the other hand, understanding of the physical characteristics and processes of Canada's northern lakes is poor, and the impact of numerous small lakes on regional weather and climate is even less well known (Spence and Rouse, 2002).

Much research on the physical climatology of lakes has focused on the variation of heat and moisture exchanges at the air-water interface. The study of a lake begins with the heat budget at its surface, and the fluxes of heat through the lake-atmosphere interface is the major source and sink for the heat involved in the thermal processes (Dutton and Bryson, 1962). Furthermore, one of the most recent studies by Mommi and Ito (2008) indicates that the study of the heat budgets of lakes is an essential component of efficient lake-water management as it gives direct information on evaporation, thus on an important component of the lakes' water budget.

Inclusion of a fully interactive lake model in the regional climate model is an important objective of the Canadian Regional Climate Modeling and diagnostics (CRCMD) network. The North American Regional Reanalysis (NARR) only considers large lakes and not small lakes in the process. Lake surfaces have very different interactions with the atmosphere, as compared to land surfaces, particularly moisture evaporation, wind forcing and energy exchanges. These air-water interactions, however, are complex and continue to be a critical issue considering the millions of lakes in Canada that are neglected in the current climatic models (Swayne et al., 2005).

In order to examine the interaction between northern lakes and surrounding regional atmosphere, Long et al. (2007) used the atmosphere-lake coupled model. The Princeton Ocean Model (POM) was coupled to the Canadian Regional Climate Model (CRCM) for Great Bear Lake and Great Slave Lake. The simulated sensible and latent heat fluxes in July and August 1999 (without and with lake) are shown in Figure 1.

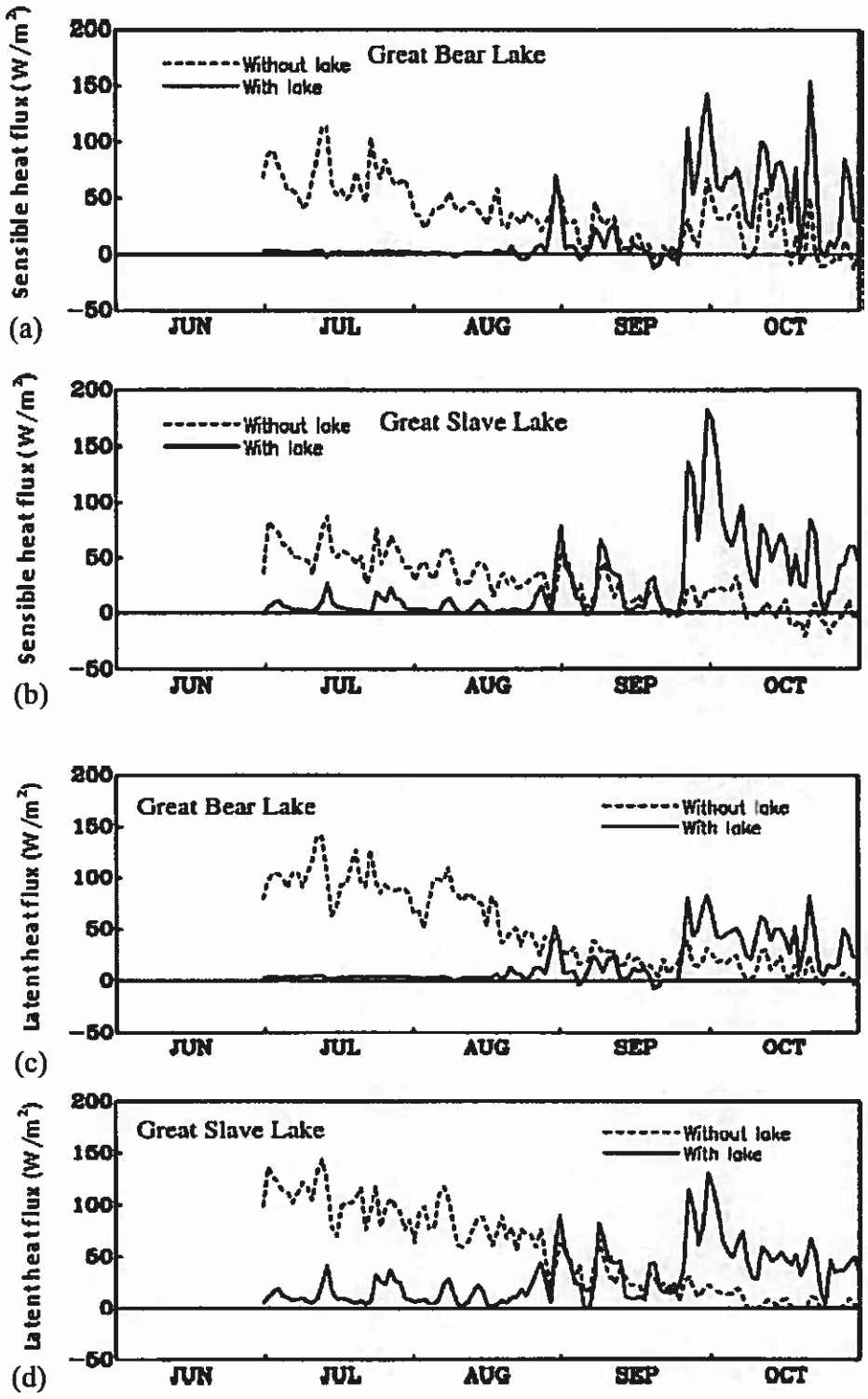

Figure 1. Lake-wide averaged sensible heat flux in 1999: (a) Great Bear Lake, (b)Great Slave Lake and averaged latent heat flux, (c) Great Bear Lake, (d) Great Slave Lake; simulations without (dashed) and with (solid) lakes (Source: Long et al., 2007)

Uncoupled simulations (without lake) result in overestimation of the surface sensible and latent heat fluxes in summer (July-August) and underestimation of these surface heat fluxes in October. The associated summer overestimation in the surface sensible heat fluxes is more than $50W/m^2$ and the October underestimation, by more than $50W/m^2$ (Figs. 1a and1b). In addition, uncoupled simulations result in a summer overestimation in latent heat transport from the lake surface (as estimated from surface evaporation), by about $100W/m^2$, and an October underestimation by about $50W/m^2$ (Figs. 1c and 1d). Therefore, the impacts of northern lakes on regional surface heat exchange between the lakes and the atmosphere are significant.

To better understand the exchange of heat and moisture between the surface and the lower atmosphere, it is important to quantify the components of the surface energy balance in a distributed fashion on the landscape scale (Segal and Arritt, 1992).

In this study sensible heat flux is quantified. Sensible heat can be used to verify climate and weather models and is necessary for regional studies of lakes and also desertification (Bolle, 1997). Accurate representation of sensible heat is beneficial to compute the heat flux in Numerical Weather Prediction (NWP), General Circulation Models (GCM) and to develop surface flux data sets (Cao et al., 2006).

Furthermore, accurate partitioning of available energy into sensible and latent heat flux (Bowen ratio) is crucial to the understanding of surface-atmosphere interaction. Bowen ratio is critical in determining the hydrological cycle, boundary layer development, weather, and climate. For example, Bowen ratio can be interpreted as an indicator of water stress.

The search for methods for estimating sensible and latent heat fluxes using low-cost, transportable and robust instrumentation constitutes a subject of interest (Castellvi et al., 2006). The measurement of turbulent fluxes requires sophisticated instruments. These measurements have been mainly confined to intensive field experiments. The direct method is expensive and complicated. When performed over a water surface, for example over a lake, these measurements are usually more difficult to obtain with great accuracy, and few direct measurements of these fluxes are available (Rouse and Spence, 2003).

Table 1 provides a list of studies related to the issue of surface flux measurement. We must emphasize that this is a representative set of previous studies, not an exhaustive list of earlier work (Jiang et al., 2004).

Because there are not enough data and meteorological stations, remotely sensed data are tools that have the potential to provide spatially distributed information. Before the advent of satellite technology, the surface fluxes, especially sensible heat fluxes and latent heat fluxes, had to be calculated exclusively relying on in situ measurements. Kampf and Taylor (2006) indicate that remote sensing is useful for identifying spatial patterns not apparent from point measurements on the ground, and it provides important insight into land surface energy budget analyses.

Therefore, understanding the energy budget of lakes and wetlands and their interaction with the atmosphere is crucial for assessing the impacts of resource development and climate changes. The current regional climate model without accounting for water components, overestimates the heat transfers when forecasts are performed in lake- or wetland-covered areas. Although several surface-based methods accurately measure surface energy fluxes at point locations, the spatial variability of the fluxes limits their application to larger spatial areas. With satellite technologies, we now have a complementary way to remotely derive surface fluxes with uniform spatial and temporal sampling.

Table 1. List of studies related to surface flux measurement derived from Jiang et al., 2004

Reference (Derived from Jiang et al.,2004)	Technique, case study or experience
Blad and Rosenberg (1974)	Bowen ratio method
Soer (1980)	Residual method for regional evapotranspiration
Kustas et al. (1989)	Residual method with thermal infrared data
Dugas et al. (1991), Fritschen et al. (1992), Kustas and Norman (1997)	Bowen ratio and eddy covariance systems
Stewart et al. (1994)	Aerodynamic formulation for H (adjusting kB^{-1})
Kustas et al. (1994)	MetFlux observation
Pelgrum and Bastiaanssen (1996)	Different methods for area-averaged λE with remote sensing data
Eichinger et al. (1996)	Priestley-Taylor method
Moran et al. (1996)	Trapezoidal method
Qualls and Brutsaert (1996)	Evaluation of ground-based and remotely sensed data to estimated spatially distributed sensible heat fluxes (FIFE measurements)
Carlson et al. (1995), Gillies et al. (1997)	"Triangle" method for soil moisture and surface fluxes from remote fluxes from remote sensing
Bastiaanssen et al. (1998)	SEBAL algorithm with remote sensing data at HEIFE
Gao et al. (1998)	Comparison of estimated Cloud and Radiation Testbed (CART) average and EBBR-derived average fluxes
Kustas et al. (1998)	Comparison between dual-source model and observations of instantaneous surface fluxes
Ibanez et al. (1998; 1999)	Radiative Bowen ratio model
Kustas et al. (1999)	Atmospheric boundary layer data and remote sensing data, N95 model
Kustas and Jackson (1999)	Impact on area-averaged heat fluxes using remote sensing data at different resolutions (Washita'92)
Mecikalski et al. (1999)	ALEXI model and Geostationary Operational Environmental Satellite 8 (GOES-8) data
Castelli et al. (1999)	Variational data assimilation approach (adjoint technique) (FIFE)
Nishida et al. (2003)	Simple two-source model of ET, combined with T–VI diagram
Norman et al. (2003)	Two-source model DisALEXI and combination of low- and high-resolution remote sensing data

1.2. Objectives

The objectives of this research are to:

- Derive sensible heat fluxes on a daily, monthly and seasonal basis as fractional values of water surfaces by combining satellite and model data at a resolution of 25 x 25 km^2.

- Analyse the impacts of northern lakes on the regional energy cycle; develop and improve the comprehensive picture of the seasonal thermal and energy regime (sensible heat fluxes) and its variability over lakes and wetlands.

- Analyse the impact of a very warm summer (1998 – the year when El Nino occurred) on the energy budget over northern areas.

- As a specific objective, we will examine the error in the energy exchange calculation between the atmosphere and land that may occur in the North American Regional Reanalysis (NARR) data due to the presence of small lakes.

1.3. Hypotheses

- To verify if the Fraction of Water Surface (FWS) modifies the surface sensible heat flux. The more the FWS increases, the more the sensible heat flux decreases, but this impact is seasonally variable. We hypothesize that this effect is more important during late summer in comparison to the early summer period.

- In the second half of the summer, the increasing sensible heat is greater than the increasing latent heat. Therefore, the Bowen ratio of the second half is greater than the first half.

1.4 Plan

The organization of the thesis is as follows: the next section describes the concept and theory of energy fluxes and turbulent energy, then the subsequent section presents the site and data descriptions of the study. The section thereafter presents the methodology. The penultimate section describes the results and hypotheses verification, and the final section contains the summary and conclusion.

2. The energy budget constraint

The turbulent fluxes of water vapour and sensible heat near the Earth-atmosphere interface are linked not only by similarity relationships in the turbulent air, but also by the energy budget. Indeed, both evaporation, as a latent heat flux, and the related sensible heat flux, require the supply of some other forms of energy. Therefore, their magnitudes are constrained by this available energy. Energy equation can be treated quantitatively by considering the energy budget for the layer of surface material. Depending on the nature of the surface, this layer may consist of water, or of some other substrate like soil, plant canopy or snow (Brutsaert, 2005).

There are essentially four types of energy fluxes at the surface:

The net radiation R_{net}: (W/m^2); sensible heat: H (W/m^2); latent heat: L (W/m^2); and the flux into or out of sub-medium soil or water: G (W/m2). The energy budget equation can be written as (Arya, 2000):

$$R_{net}=H+L+G \qquad (1)$$

The sensible heat flux (H) at and above the surface arises as a result of the difference in the temperatures of the surface and the air above. In the case of sensible heat transfers, a temperature gradient must exist between the surface and the subsurface for a heat transfer to occur (Arya, 2000).

Sensible heat fluxes in lake surfaces play an important role in the energy balance between lakes and the atmosphere. The sensible heat flux is the direct physical contact of the atmosphere and lake, and enables energy to be exchanged between them by conduction (Bigg, 1996).

Through sensible heat fluxes, the lake absorbs (releases) the heat energy from (to) the atmosphere, compensating for the sharp temperature change in the atmosphere and adjusting the local climate and beyond (Pan et al., 2003).

We used the sign convention that all the radiative fluxes directed towards the surface are positive, while other (non radiative) energy fluxes directed away from the surface are positive. Figure 2 shows the sensible heat flux away from (positive) and toward (negative) the surface.

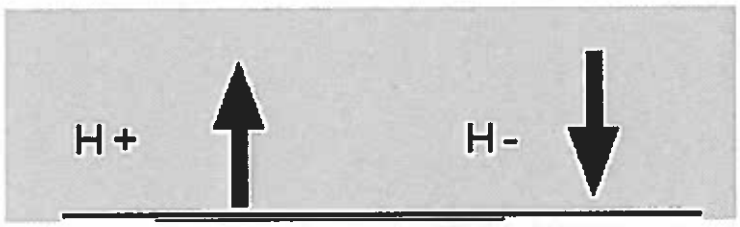

Figure 2. Direction of sensible heat fluxes

The latent heat flux (L) is a result of evaporation, evapotranspiration or condensation, and the rate of evaporation or condensation at the surface. Evaporation occurs from water surfaces as well as from moist soil and vegetation surfaces whenever the air above is drier, i.e., it has lower specific humidity than the air in the immediate vicinity of the surface and its transpirating element (Arya, 2000).

The ground heat flux (G), to or from the sub-medium and heat, is transferred via conduction (Arya, 2000). This flux is a small, but not insignificant, component of the surface energy budget. This flux is also related to the surface temperature (Stull, 1998).

The net radiation (R_{net}) absorbed by the surface is the sum of the net shortwave (solar) and long wave (thermal) radiations:

$$R_{net} = (S_{\downarrow} - S_{\uparrow}) + (L_{\downarrow} - L_{\uparrow}) \qquad (2)$$

$S_{\downarrow}$ and $S_{\uparrow}$ are the respective incoming and outgoing (or reflected) shortwave radiations, and $L_{\downarrow}$ and $L_{\uparrow}$ are the respective incoming and outgoing long wave radiations (Arya, 2000). Figure 3 shows a schematic figure of the heat budget near the surface. The energy incoming into a layer adjacent to the ground, the so-called available energy (R_{net} – G), must be divided between sensible heat (H) and latent heat (L) energy (Manilo, 1989).

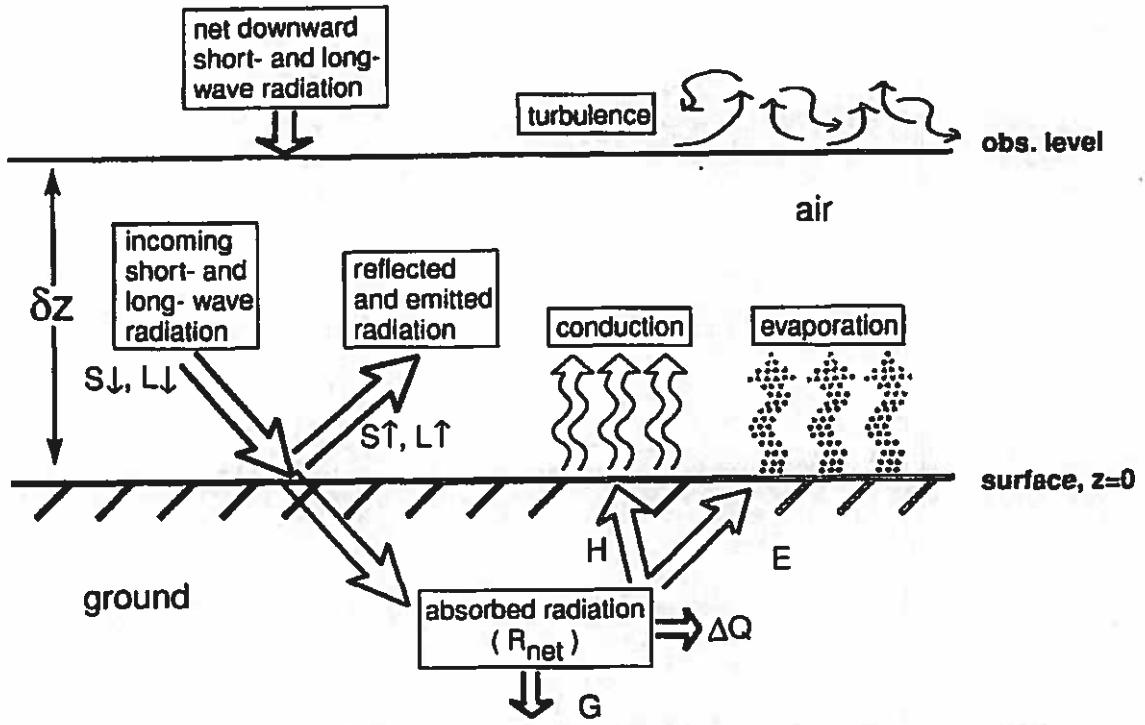

Figure 3. Schematic figure of the heat budget of a thin interfacial layer near the surface (Source: Sun et al., 1995)

3. Site description

Four different vegetation types were selected for this study, ranging from mature forest to tundra. Figure 4 shows the locations of the sites. The four sites used in this study are as follows:

The first site is some parts of Great Slave Lake (GSL) and Mackenzie River Basin (MRB) in the Northwest Territories. Lackman and Gyakum (1996) reported that evaporation over the MRB exceeds adjective transport of moisture during the summer season, suggesting that the MRB is in itself a significant source of moisture and a suitable place for orographic or lee-cyclogenesis and front genetic processes which influence the east of Canada. The dominant land cover type at this site is boreal forest. This thesis refers to the site as "GSL."

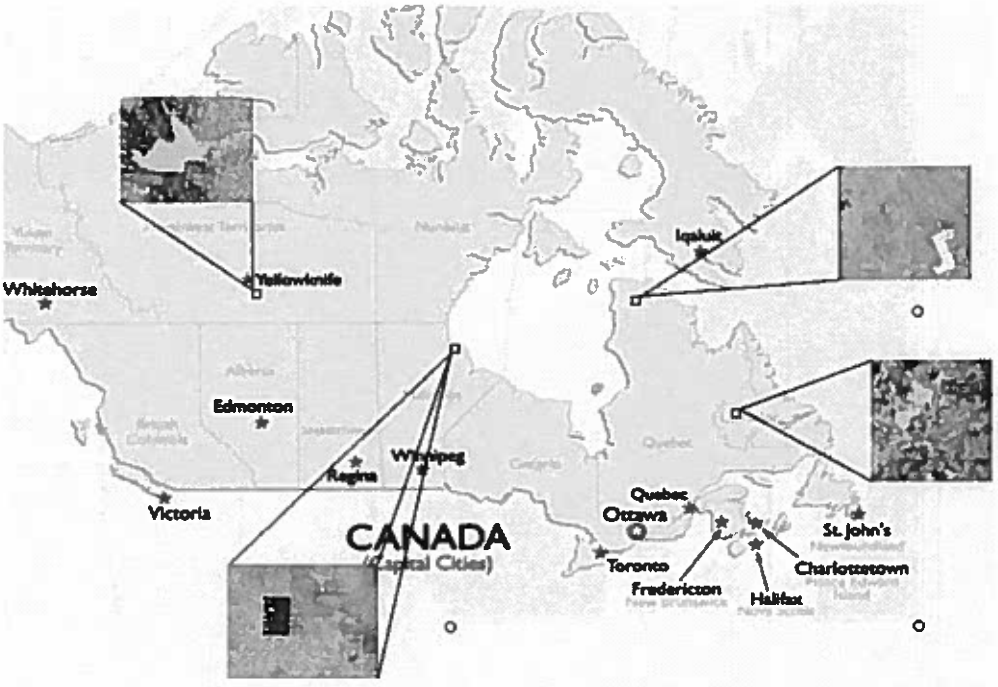

Figure 4. Location of the study sites

The second site is located in northern Manitoba, south of Hudson Bay. This region is characterized by dominance of wetland areas. Understanding the energy exchange of wetlands is important because it affects radiative and temperature regimes, water transport, plant growth, and productivity (Burba et al., 1999). This thesis refers to this site as "Wetland."

The third site is located in north-western Labrador. The area is very important in the field of hydrology, and this region is characterized as Taiga (open forest), Tundra and a number of small bodies of water. The thesis refers to this site as "Taiga."

The fourth site, located in the northern Quebec, is covered with tundra. The tundra area has a unique water cycle due to the presence of frozen ground (Kodama et al., 2007). The distribution of low vegetation, such as lichens, moss, and sedge, also plays an important role in surface energy over the tundra watershed (Sato, 2004). This research refers to this site as "Tundra." The geographical coordinates of the sites are given in Table 2.

Table 2. The geographical coordinates of the study sites

Location	Dominant land cover type	Lat		Lon	
		N	S	W	E
Northwest Territories	Boreal forest	64.492	60.989	115.968	111.96
Manitoba	Wetland	59.043	58.043	95.455	93.344
Labrador	Taiga	54.505	53.470	65.485	62.988
Quebec	Tundra	61.045	59.962	74.985	71.934

4. Data description

The estimation of surface sensible heat fluxes can be accomplished through several methods. Most of these methods usually require key input parameters such as air

temperature, wind speed and surface temperature (Stull, 1988). Furthermore, estimation energy flux requires the combination of data from several sources. In this study, there are three essential sources of data.

The first source is the remote sensing. We used the data provided by the Special Sensor Microwave Imager (SSM/I). The SSM/I is onboard the Defence Meteorological Satellite Program (DMSP), a satellite series that visits the same part of the Earth's surface twice a day. Passive microwave measurements are independent of solar illumination, and information from the surface can be acquired even through clouds as opposed to optical sensors (Fily et al., 2003).

The pixel spatial resolution depends on the frequency measured. However, in the re-sampled Northern Hemisphere Equal Area Scalable (EASE-Grid) format, the data are readily available at a resolution of 25 km. These data are distributed by the National Snow and Ice Data Center (NSIDC), located in Boulder, Colorado (USA). Our research is restricted to the 19.35 and 37 GHz frequencies, as they are less affected by atmospheric effects. Only the 37 GHz are used from this point on because the penetration depth is smaller than it is for the 19.35 GHz channel, making it sensitive to soil moisture, and because the spatial resolution at this frequency is closer to the EASE-Grid resolution: 27 km x 18 km at 37 GHz as opposed to 69 km x 43 km at 19.35 GHz. In addition, we used the land-cover database of North America for the year 2000. It is generated jointly by the Canada Centre for Remote Sensing (Natural Resources Canada) and the US Geological Survey. It was compiled using SPOT VEGETATION data at the spatial resolution of 1 km land-cover type.

The second source of data is the North American Regional Reanalysis (NARR). The North American Regional Reanalysis is a reprocessing of the historical meteorological observations using National Centers for Environmental Protection NCEP's regional climate model. The NARR project was completed in 2004. NARR products are in GRIB format on a Lambert conformal conic grid (32 km) at 29 pressure levels.

They were produced using a 45-layer topography model. The NARR is a long-term, dynamically consistent high-resolution, high-frequency atmospheric and land surface hydrology dataset for North American domain (Mesinger et al., 2006). The output analyses are 3-hourly with 9 additional variables in the 3-hour forecasts to reflect accumulations or averages.Finally, we used an Eco-forestry map in order to find the canopy height. Figure 5 shows briefly data and acquired sources.

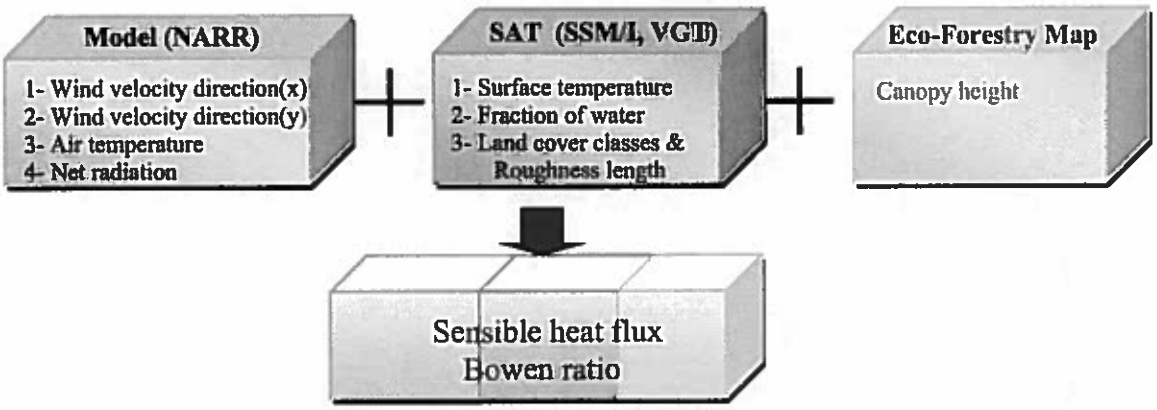

Figure 5. A quick view of the data and acquired sources

5. Methodology

Based on satellite remote sensing data (SSM/I and SPOT VGT sensors), the NARR model and the atmospheric boundary layer, the methodologies to determine sensible heat fluxes and the Bowen ratio are deduced. Figure 6 shows the algorithm used for this study.

The methodology is divided into two essential parts: the first part is data processing and the second part is retrieval processing.

5.1 Data processing

In this part we extracted surface temperature, FWS, atmospheric temperature, wind speed, net radiation, and land surface characteristics:

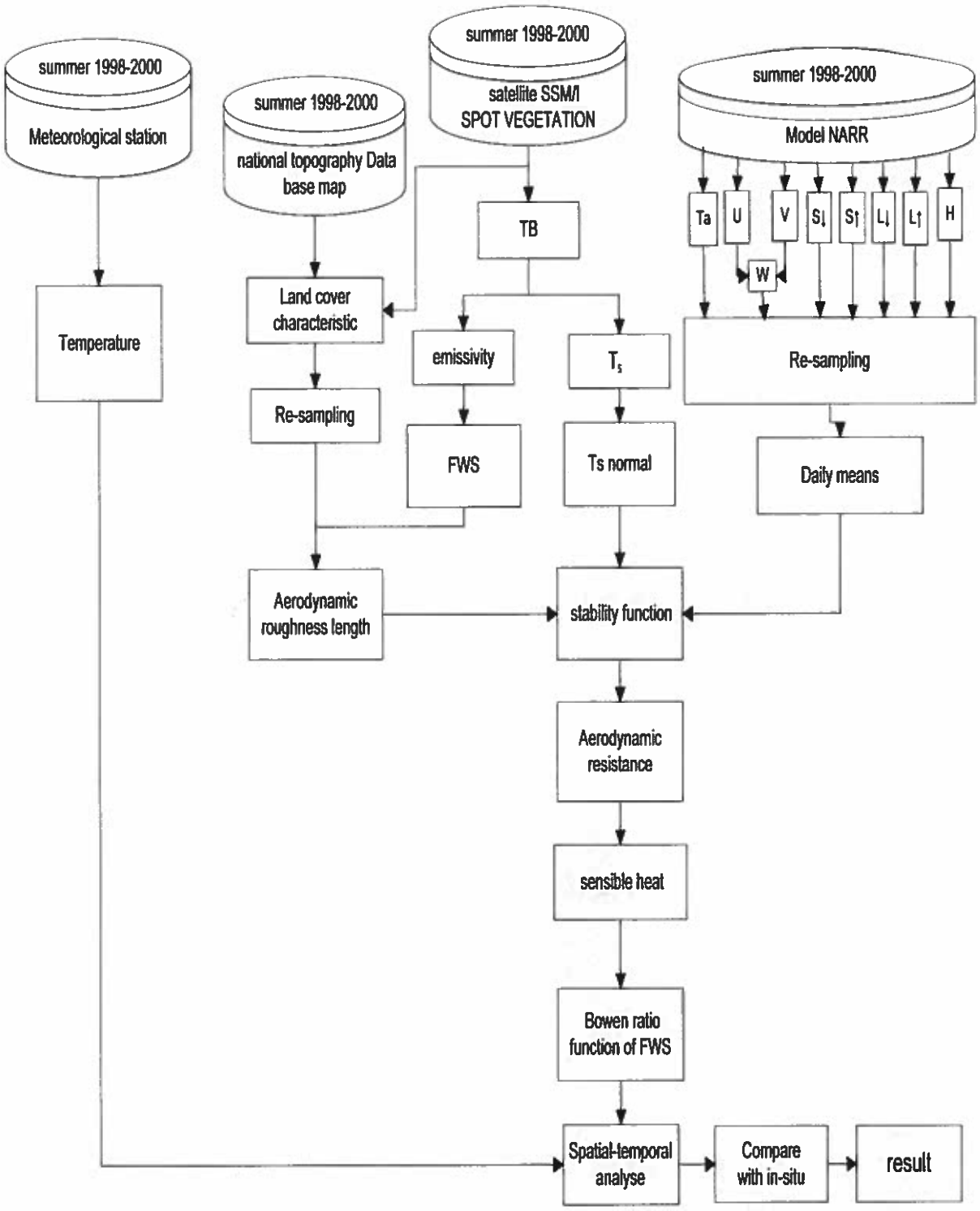

Figure 6. Flowchart used for the study

5.1.1 Temperature derived from satellite measurements

At a given polarization *p*, for any frequency, the apparent brightness temperature TB_p at satellite level can be written (Fily et al., 2003):

$$TB_p = ep \times t \times T_s + (1 - ep) \times t \times T_{ab} + T_{au} \qquad (3)$$

Where *ep* is emissivity at polarization *p*, *t* is atmospheric transmission, T_{ab} is downward atmospheric contribution, T_{au} is upward atmospheric contribution, T_s is land surface temperature.

Brightness temperature consists of gridded data in an EASE-Grid projection. They are provided at a 25 km resolution at a given location in our station area: up to two measurements per day are available.

5.1.2 Determination of Fraction of Water Surface (FWS)

Assuming a linear relationship between emissivity at vertical polarization (e_v) and emissivity at horizontal polarization (e_H)as suggested by Fily et al. (2003) such as $e_v = ae_H + b$ (a=0.5022 and b=0.4838 at 37 GHz) .we can eliminate the unknown emissivity from the relation (3), the surface temperature is (Fily et al., 2003):

$$T_s = \frac{(TBV - a \times TBH - (1 - b - a) \times t \times T_{ab} \times T_{au} \times (1 - a))}{(t \times b)} \qquad (4)$$

Where TBV and TBH are the apparent brightness temperature at polarization vertical and horizontal respectively. We then obtain two sets of temperatures (T_s - 19 and T_s - 27), one for each frequency; from Equation 4, the emissivity can be computed as:

$$ep = \frac{(TB_p - t \times T_{au} - T_{ad})}{(t \times (T_s - T_{ad}))} \qquad (5)$$

And finally, the fraction of water surface (FWS) in the observed pixel (Fily et al., 2003):

$$FWS = \frac{(ep - edry)}{(ew - edry)} \qquad (6)$$

where *edry* is the emissivity of a dry surface and *ew* is the emissivity of water. The FWS includes surface bodies of water, saturated wetland swamps, marshes, or fens. Therefore, based on Fily et al. (2003), the FWS values are aggregated at a 25 x 25 km pixel resolution on the EASE-Grid geographical projection.

5.1.3 Satellite-derived temperature daily normalization

Remote sensing images record a snapshot in time, whereas land surface energy fluxes change continuously. In this study, since a maximum of only two temperatures can be derived daily from satellite overpasses, it is difficult, it is difficult to compare satellite-derived temperatures with other climatic sources based on mean daily. In order to obtain the daily mean surface temperature, the method proposed by Mialon (2007) was used to extract the Normalized Surface Temperature (NST).

A normalization approach based on the 40-year ECMWF reanalysis (ERA-40; 2.5° resolution) temperature diurnal cycle fitted for each pixel is applied to overcome the time acquisition variation of measurements as well as to interpolate missing data. An adaptive mask for discriminating between ice-free pixels and snow-free pixels is also applied. The resulting database is thus a new consistent hourly series of near-surface air temperatures during the summer (without snow). For consistent time series, it is necessary to accurately interpolate the gaps between measurements by taking into account the diurnal cycle(Mialon et al 2007).

ERA-40 air temperatures are available every 6 h at a spatial resolution of 2.5°. An hourly diurnal cycle is obtained from ERA-40 data interpolated with a spline cubic function (Mialon et al., 2005).

This interpolation technique has the advantage of producing smooth series at measurement points. The principles of this approach are presented in Figure 7. One or two ΔT (i.e. T_{sat} minus ERA-40 temperature interpolated at a given hour) are available every day. A linear interpolation is then used to obtain hourly ΔT series. Adding hourly ΔT series to hourly ERA-40 temperature series results in an hourly temperature series (hereinafter referred to as normalized temperature $T_{sat,\ norm}$) fitted with satellite-derived temperatures from Equation 4 (Mialon et al., 2005).

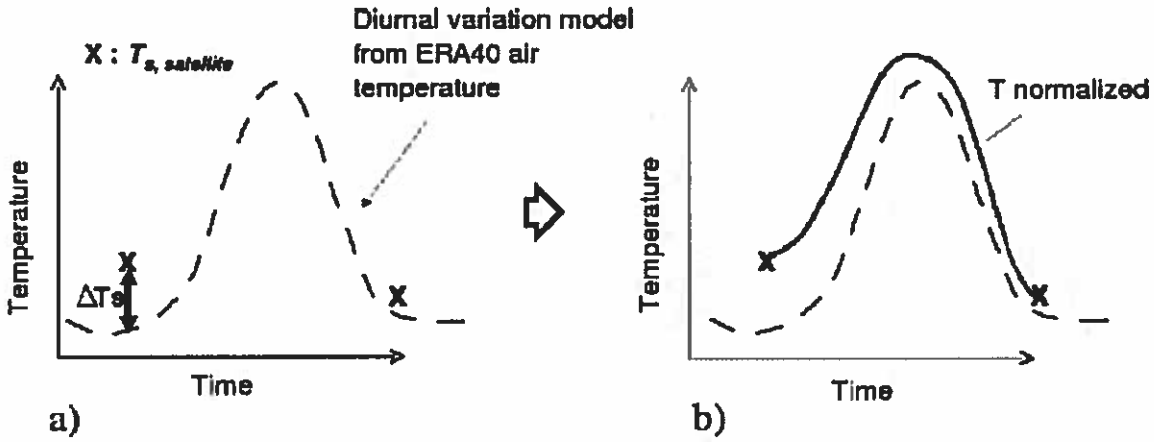

Figure 7. Normalization process: applying ERA-40 diurnal cycle (dashed line) to satellite-derived temperature (x) derived from SSM/ I sensor leads to normalized (hourly) series (solid line)

5.1.4 Image processing

The estimation of sensible and latent heat fluxes typically requires knowledge of land cover characteristics and surface states (Bertoldi et al., 2008). Different land covers will have unique surface roughness and thermal characteristics, which affect the sensible and ground heat flux (Kampf and Taylor, 2006). In this part we used the "Land cover database of North America" for the year 2000. It is produced jointly by the Canada Centre for Remote Sensing (NRCan) and the US Geological Survey (Latifovic et al., 2002). It includes 29 classes (See Appendix B). In the present study, we will focus on 6 classes, as follows: 1-sub-polar mixed broadleaved or Needleleaved Forest, 2-

Shrubland, 3-grassland, 4-Cropland, 5-lichen and sparse vegetation, and 6-Water bodies.

We changed the resolution and projection on EASE-Grid for a resolution of 25 km. This way we were able to determine the percentage of classes for each pixel at 25 x 25 km (Köhn, 2006). Figure 8 shows the results on the EASE-Grid projection.

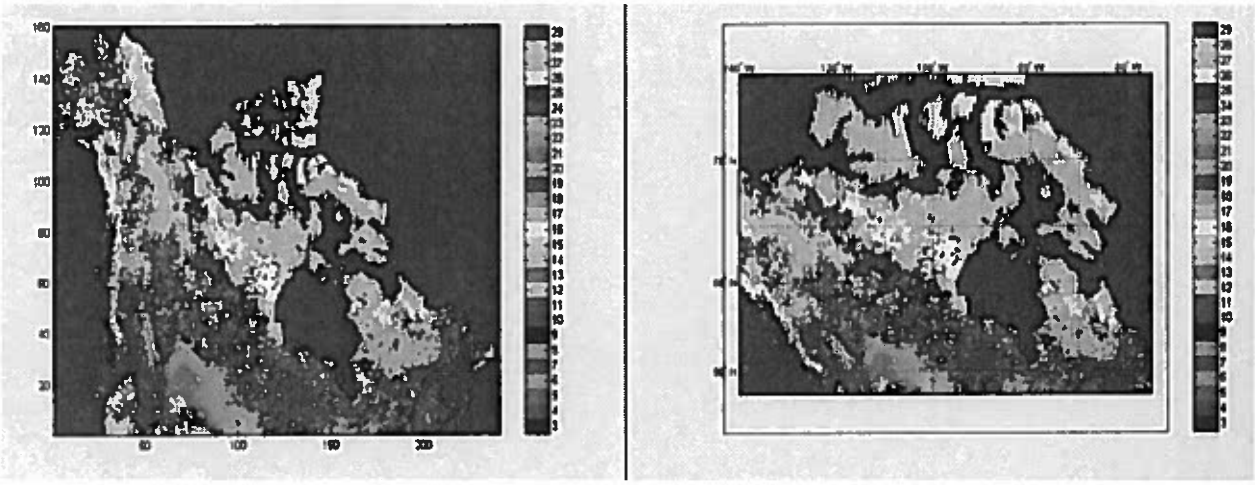

(a) (b)

Figure 8. Land cover classification of North American year 2000 (Latifovic et al., 2002) (a) EASE-Grid projection and (b) visualization of the same figure in geographical coordinates

5.1.5 Extraction of the NARR data

The wind components in *x* and *y* directions (U and V respectively), were acquired from the NARR at a 32 km resolution. After re-sampling and projected on EASE-Grid (25 km), the wind speed (W) was calculated as follows (Holton, 2004):

$$W = (U^2+V^2)^{1/2} \quad (7)$$

In addition to wind components, upward long radiation, downward long radiation , upward short radiation , and downward short radiation are obtained from the NARR model at a 32 km resolution. After re-sampling and projected on EASE-Grid, net

radiation was calculated by relation (2). In order to compare the retrieved result with modelled; the sensible heat flux was extracted.

The NARR air temperature (at 10 m above ground) is used for the satellite-based retrieved sensible heat flux. It is assumed that this value depends primarily on atmospheric conditions given by the model and then T_a is little linked to the land cover (at the second order). It is then justified to use the NARR data (T_a, W, R_{nct}).

5.2 Retrieval of sensible heat flux from satellite data

On the ground, sensible heat flux is typically determined from high frequency wind speed and air temperature measurements (eddy correlation technique). For remote sensing application, the sensible heat flux can be calculated based on the surface-air temperature gradient and on aerodynamic resistance (Kampf and Tyler, 2006).

The method of resistance is a combination method of energy balance, the relation between fluxes and gradients of mean quantities and an a priori evaluation of surface conditions. The general form is (Berkowice and Prahm, 1982):

$$\text{Flux} = \frac{\text{Potential difference}}{\text{resistance}} \qquad (8)$$

Depending on which quantity the flux refers to, the potential difference corresponds to the proper parameter. Thus, when the flux of heat is considered, the potential difference refers to temperature difference.

5.2.1 Retrieval of sensible heat flux

The sensible heat flux H (W/m^2) can be defined using the bulk resistance in a fashion analogous to Ohm's Law (Monteith, 1973). Figure 9 shows the schematic general form of the theory:

$$H = \rho C_p \frac{T_s - T_a}{r_a} \qquad (9)$$

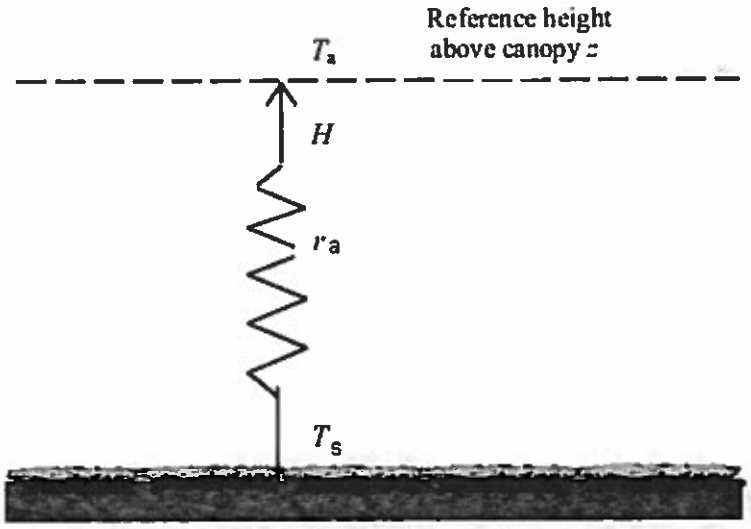

Figure 9. Schematic description of model for heat transfer (Source: Lia, 2004)

The regional distribution of sensible heat flux is expressed as follows (Ma and Ishikawa, 2003):

$$H(x,y) = \rho C_p \frac{T_s(x,y) - T_a(x,y)}{r_a(x,y)} \qquad (10)$$

Where ρ is the air density(kgm^{-3}), C_p is the specific heat of the air (Jkg^{-1}k^{-1}), T_s is the surface temperature (°K) obtained from the SSM/I, T_a is the air temperature (°K) obtained from the NARR model, r_a is the aerodynamic resistance (sm^{-1}) determined by the Monin-Obukhov surface layer similarity theory, as follows:

$$r_a(x,y) = \frac{1}{ku*(x,y)}\left[\ln\left(\frac{Z - d_0(x,y)}{Z_0(x,y)}\right) + kB^{-1} - \psi_h(x,y)\right] \qquad (11)$$

Where k is Von-Karman's constant and its empirical constant with a value of about 0.40 (Hogstorm, 1985), while $u*$ is the friction velocity (m/s), expressed as follows (Ma and Ishikawa, 2003):

$$u^*(x,y) = kW(x,y)\left[\ln\left(\frac{Z - d_0(x,y)}{Z_0(x,y)}\right) - \psi_m(x,y)\right]^{-1} \quad (12)$$

Where $W(x, y)$ is the wind speed (m/s) obtained relation (7). Z (Reference height = 10 m) is the height of the wind speed observed (Stull, 2000), $Z_0(x, y)$ is the aerodynamic roughness length (m), roughness length is defined by the logarithmic wind profile, and is valid in the lower part of a neutrally stratified boundary layer (Dejong et al., 1999), and it is determined based on land cover classes. The value of Z_0 depends on the characteristics of the surface (See Appendix 2) ranging from a value of 0.001 cm over smooth ice to 10 m over large buildings (Oke, 1978). d_0 is the zero-plane displacement height (m), which is proportional to the canopy height, as shown in the following (Quattrochi and Luvall, 2004):

$$d_o(x, y) = 2/3\ h_c(x, y) \quad (13)$$

where h_c is the canopy height (m), and is determined by the Eco-forestry map. The added resistance term $KB^{-1} \approx 2$ (Garratt and Hicks, 1973), B^{-1} is a non-dimensional bulk parameter, KB^{-1} taking into account the fundamental difference in the mechanisms determining heat and momentum transfer (Thom, 1972).

ψ_h and ψ_m are the stability correction functions (dimensionless) for heat and momentum transfers, respectively. The stability correction functions are related to the stability condition of the atmosphere, which is characterized by the dimensionless Richardson number R_i (Businger, 1988):

$$Ri(x,y) = \frac{5 \cdot g(Z - d_0(x,y))(T_s(x,y) - T_a(x,y))}{W(x,y)^2\left(\left(\frac{T_s(x,y) + T_a(x,y)}{2}\right) + 273.16\right)} \quad (14)$$

where g is the acceleration due to gravity (m/s^2), Z is the reference height (m), $d(x, y)$ the zero displacement height (m), Ts(x, y) the surface temperature (°K), Ta(x, y)

atmospheric temperature (°K), *W(x, y)* is the wind speed (m/s). To determine correction functions, we first calculated R_i (x, y).

Normal conditions exist when Ri = 0, corrections functions are as follows (Stull 1998):

$$\psi_m(x,y) = 0 \quad \text{and} \quad \psi_h(x,y) = 0.64 \qquad (15)$$

For unstable conditions (R<0), the stability correction functions can be determined using the Businger-Dyer formulations (Businger, 1988; Sugita et al., 1990), which yield the following expressions:

$$\psi_m = 2\ln\left(\frac{1+x}{2}\right) + \ln\left(\frac{1+x^2}{2}\right) + 2\arctan(x) + \frac{\pi}{2} \qquad (16)$$

$$\psi_h = 2\ln\left(\frac{1+x^2}{2}\right) \qquad (17)$$

For stable (R>0) conditions (Webb 1970)

$$\psi_m = \psi_h = -5\xi \qquad (18)$$

Where $x = (1-16\zeta)^{1/4}$ and $\zeta = (z_r - d)/L_o$, in which L_o is the Obukhov stability length. The stability factor ξ can be replaced by the Richardson number (Ri) using the following relationships (Thom, 1975; Businger, 1988):

$$R_i = \begin{cases} \xi & \textit{Unstable} \\ \dfrac{\xi}{1 + 5\xi} & \textit{Stable} \end{cases} \qquad (19)$$

Combining Equations (10), (11), (12) yields:

$$H(x,y) = \rho C_p k^2 W(x,y) \frac{T_S(x,y) - T_a(x,y)}{\left[\ln\left(\frac{Z - d_0(x,y)}{Z_0(x,y)}\right) + KB^{-1} - \psi_h(x,y)\right] \cdot \left[\ln\left(\frac{Z - d_0(x,y)}{Z_0(x,y)}\right) - \psi_m(x,y)\right]} \quad (20)$$

5.2.2 Estimation of Bowen Ratio

The energy balance equation (1) can be written as follows:

$$R_{net}(x, y) - G(x, y) = L(x, y) + H(x, y) \quad (21)$$

Ground heat flux (G) is assumed negligible in this study (mean daily budget), so the latent heat flux was retrieved as follows:

$$L(x, y) = R(x, y) - H(x, y) \quad (22)$$

The partition of energy between sensible (H) and latent heat (L) flux is usually obtained by the Bowen ratio-energy balance method (Tanner et al., 1987; Kustas et al., 1996) by means of the Bowen ratio:

$$\beta(x, y) = H(x, y) / L(x, y) \quad (23)$$

The Bowen ratio (β) is a dimensionless quantity which measures the ratio of sensible to latent heat-flux densities and can be expressed as being proportional to the ratio of air temperature increment to vapor pressure increment over a finite height interval. Such a quantity is important to understand because knowledge of this variable quantifies the relative magnitudes of surface energy expenditure to heat the air and to evaporate water, and has been used widely in evaporation estimation (Revfeim and Jordan., 1976).

.

5.3 Temperature condition

Atmospheric temperatures of meteorological stations which were close to each site were considered as representative of the temperature conditions during the estimated period. Table 3 shows the names of stations which are close to our study sites and the conditions for the two years considered as compared to the 1971-2000 normal (See Appendix 3).

Table 3. Name of sites and close meteorological stations

Site	Name of station	Year 1998	Year 2000
GLS	Yellowknife	Above normal	Normal
Wetland	Churchill	Above normal	Normal
Taiga	Churchill Falls	Normal	Above normal
Tundra	Kuujjuaq	Above normal	Above normal

6. Results

This section presents the results of a concerted effort to compare the retrieved data on sensible heat at various sites in northern Canada with the results of modelling studies for the regions. The results from this study present a picture of the daily, monthly and seasonal behaviour of sensible energy over two summers (1998 and 2000) at the land-air interface.

6.1 Comparison between retrieved and modelled sensible heat flux

Figures 10, 11, 12, and 13 show the 3-dimensional variation of sensible heat flux as a function of FWS(%)and day in July and August 1998-2000 for the GSL site. The modelled results show there are larger variations for less than 25% FWS and more than 70% FWS. However, when the FWS is between 25% and 70%, the modelled results indicate low variations. On the other hand, retrieved results show more variations of sensible heat flux for the range between 25% and 70%.

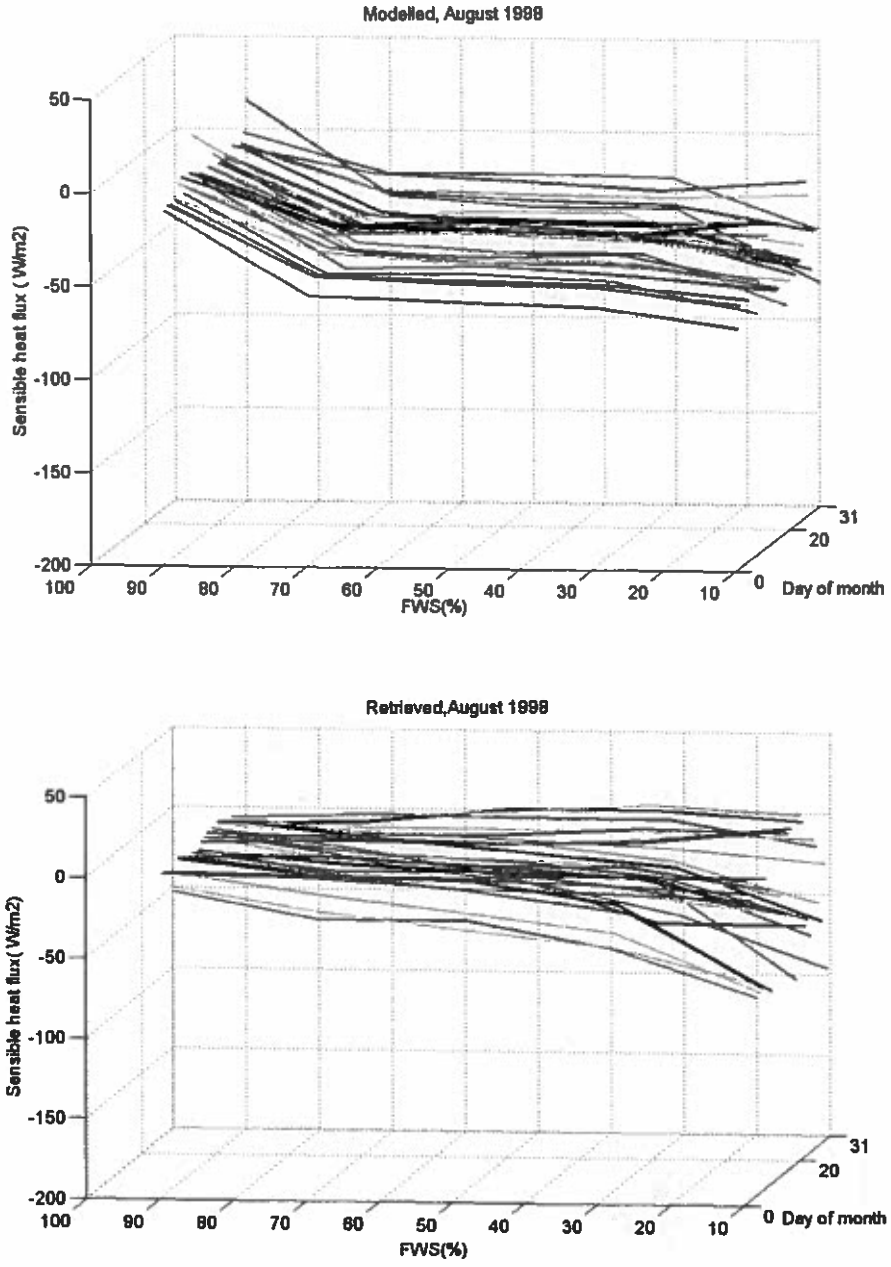

Figure 10. The daily variation of sensible heat as a function of FWS for the GSL site - August 1998*

*Each line represents one day of the month.

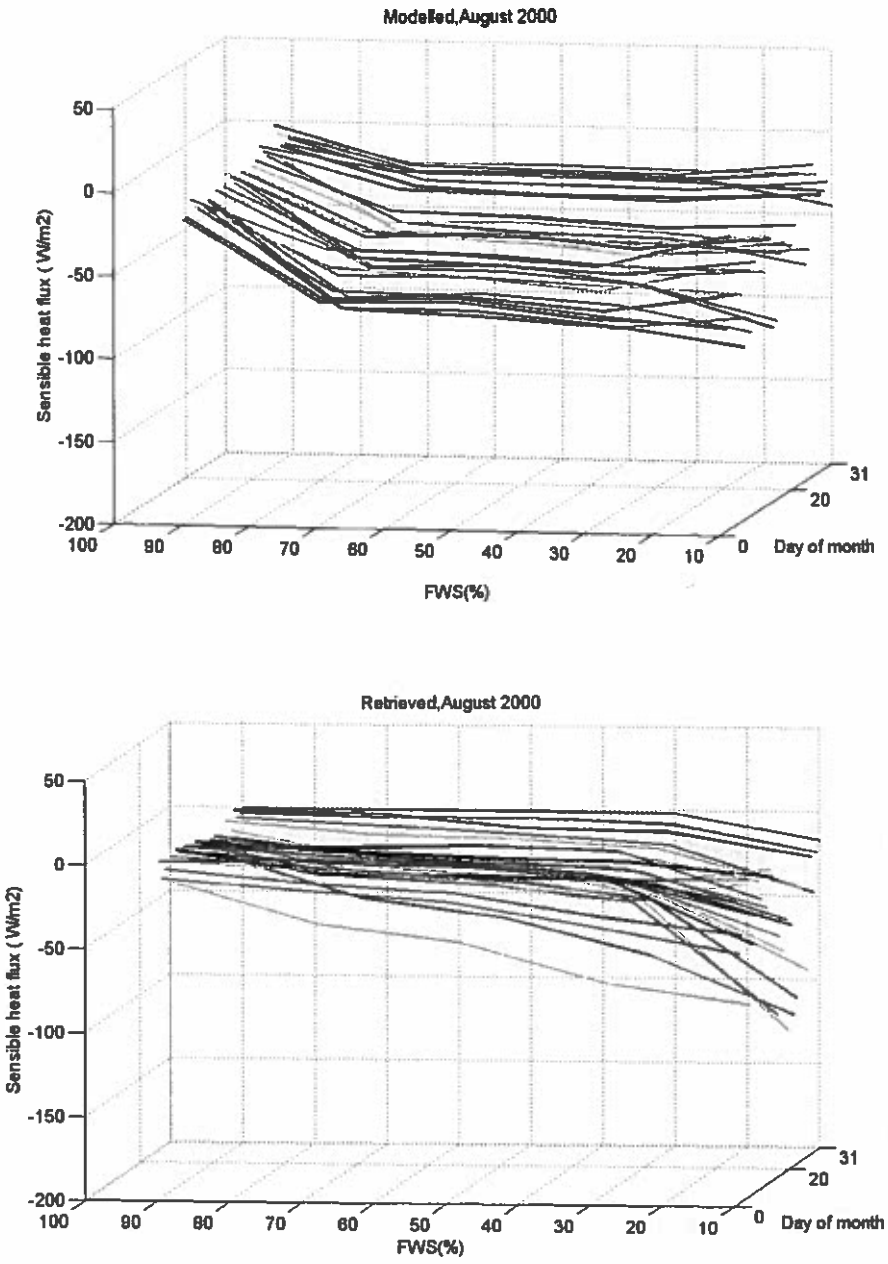

Figure 11. The daily variation of sensible heat as a function of FWS for the GSL site - August 2000*

*Each line represents one day of the month

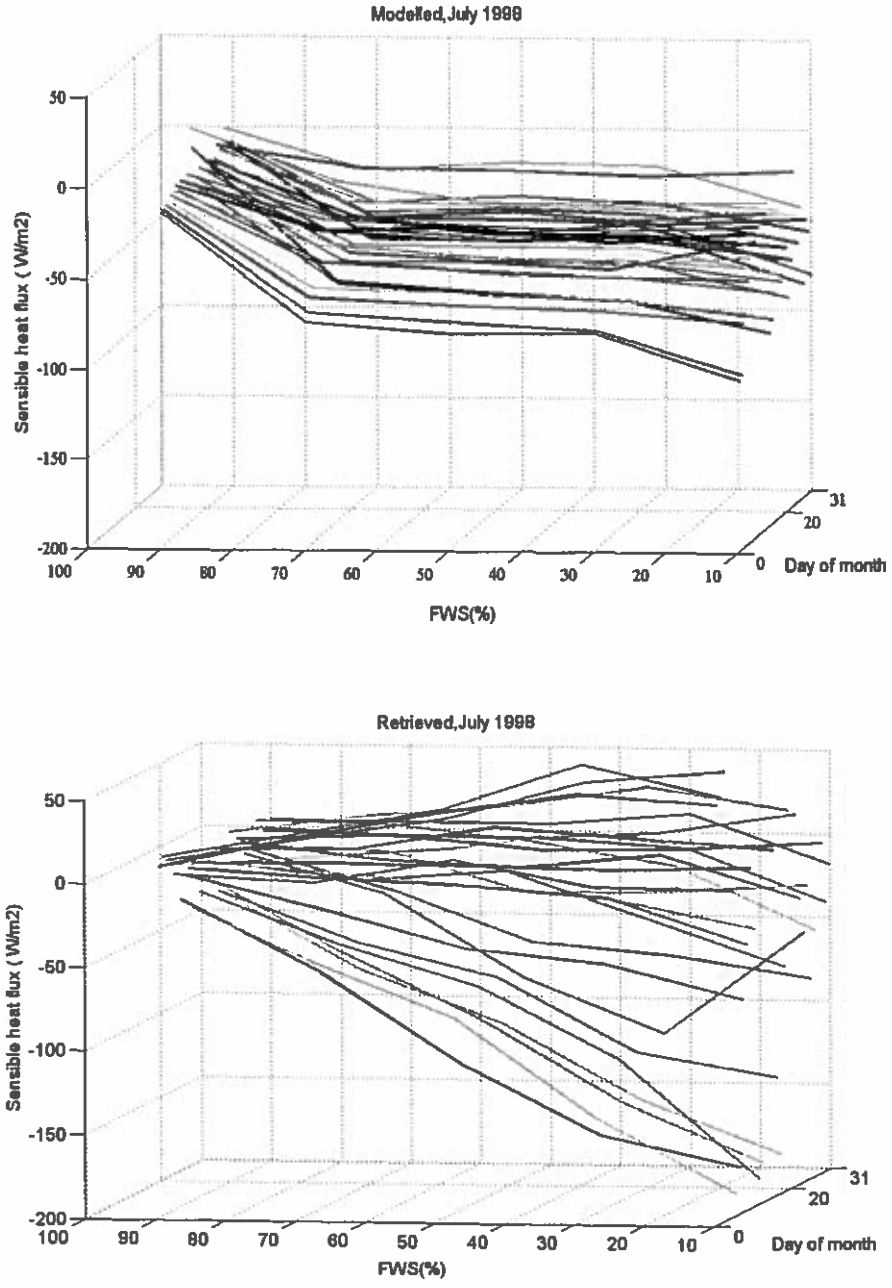

Figure 12. The daily variation of sensible heat as a function of FWS for the GSL site - July 1998*
*Each line represents one day of the month.

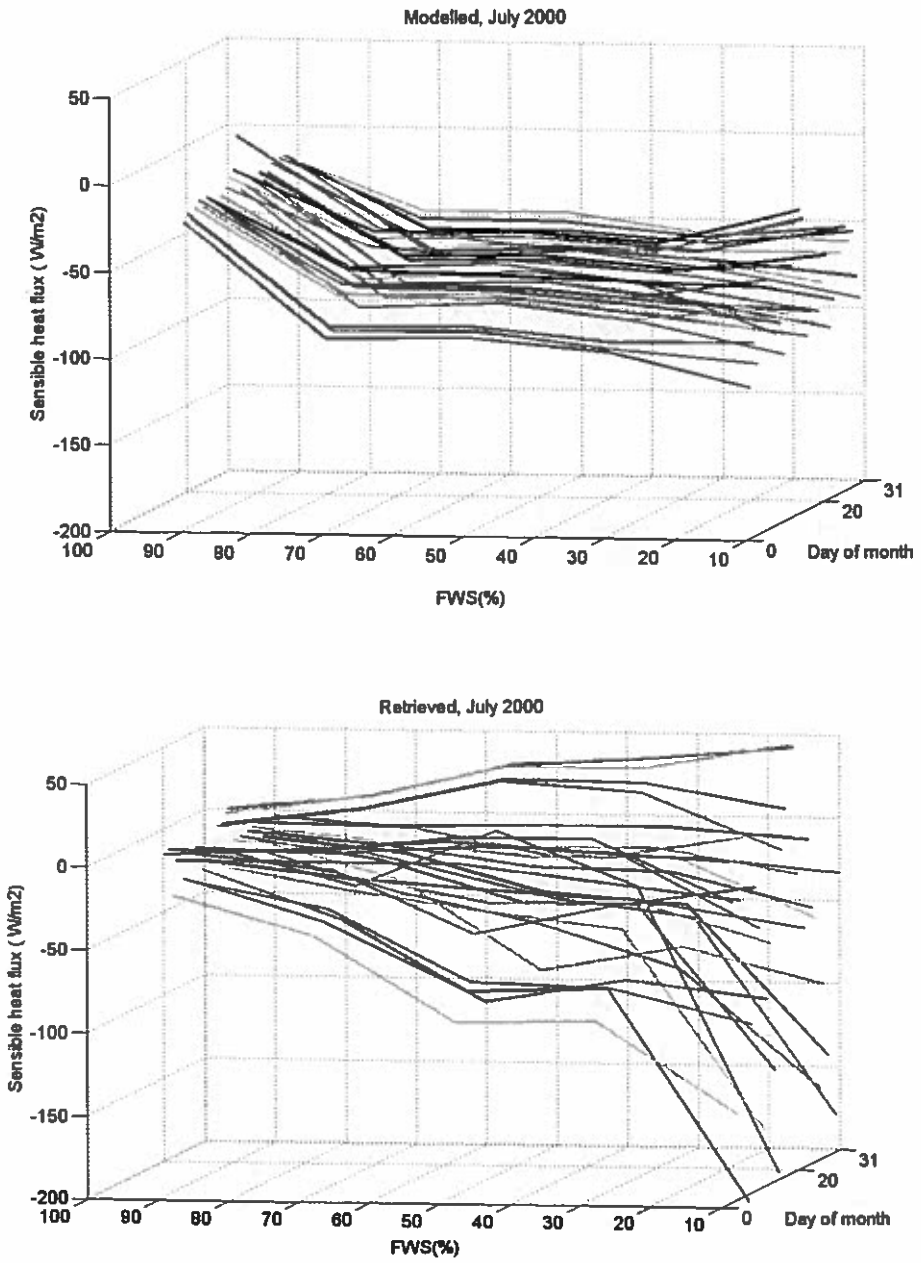

Figure 13. The daily variation of sensible heat as a function of FWS for the GSL site - July 2000*

*Each line represents one day of the month.

In order to evaluate the performance of the NARR model for different fraction values of water surfaces, we computed the retrieved and modelled sensible heat fluxes for the monthly mean and standard deviation against FWS during the summer months. Error bars reflect the variance of sensible heat versus FWS for retrieved and modelled results.

For this purpose, we divided FWS into 5 equal intervals (1-20, 21-40, 41-60, 61-80, and 81-100% FWS). Then, monthly mean sensible heat fluxes and standard deviation for the pixels situated in each interval are calculated separately. Figure 14 shows the monthly mean of sensible heat versus FWS for the GSL site. It should be noted that for the GSL site in 2000, the month of June is incomplete. Because of the snow cover in the first half of the month, only the second half was processed.

For the GSL site, the two intervals (1-20% and 81-100% FWS) both results overlap (same mean values), meaning that there are no significant differences between the modelled and retrieved values for the area with no lake and the area covered with large lakes. On the other hand, for 20% < FWS < 80% values, there are fewer overlaps between the modelled and retrieved error bars. This indicates that there are more differences (in comparison) between the retrieved and modelled values over areas partially covered by water bodies.

Figure 15 shows the monthly mean of sensible heat versus FWS for the Wetland site. As the figure shows, for this site the modelled mean values are always higher (high negative values) than the retrieved satellite-based sensible heat flux (positive values). This could mean that the model does not take into account the land cover type. As a matter of fact, water bodies (small lakes and wetlands) remain warmer in August and September than the air. This leads to positive sensible heat flux for areas having high fraction of water surface. If the model does consider neither wetlands nor small lakes, it will calculate a high negative (downward) sensible heat flux, so the partition of sensible heat will be increased and the partition of latent heat decreased. On the other hand, the retrieved values which are based on high sensitivity to fractional water surfaces show

less value for sensible heat flux (the partition of sensible is decreased so the partition of latent will be increased).

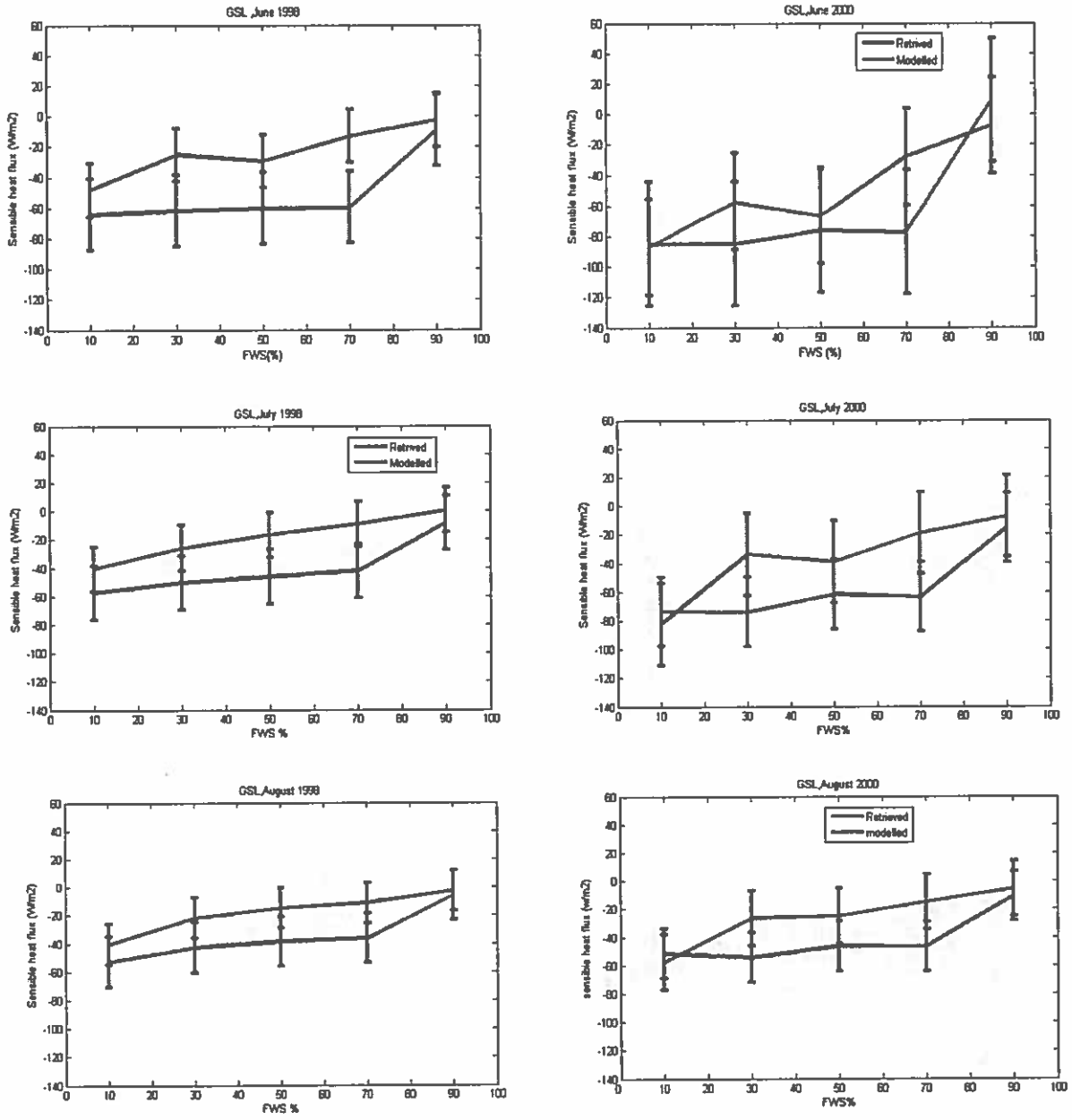

Figure 14. Average sensible heat flux versus FWS*%, GSL

*The length of the vertical bars indicates twice the standard deviation for each interval.

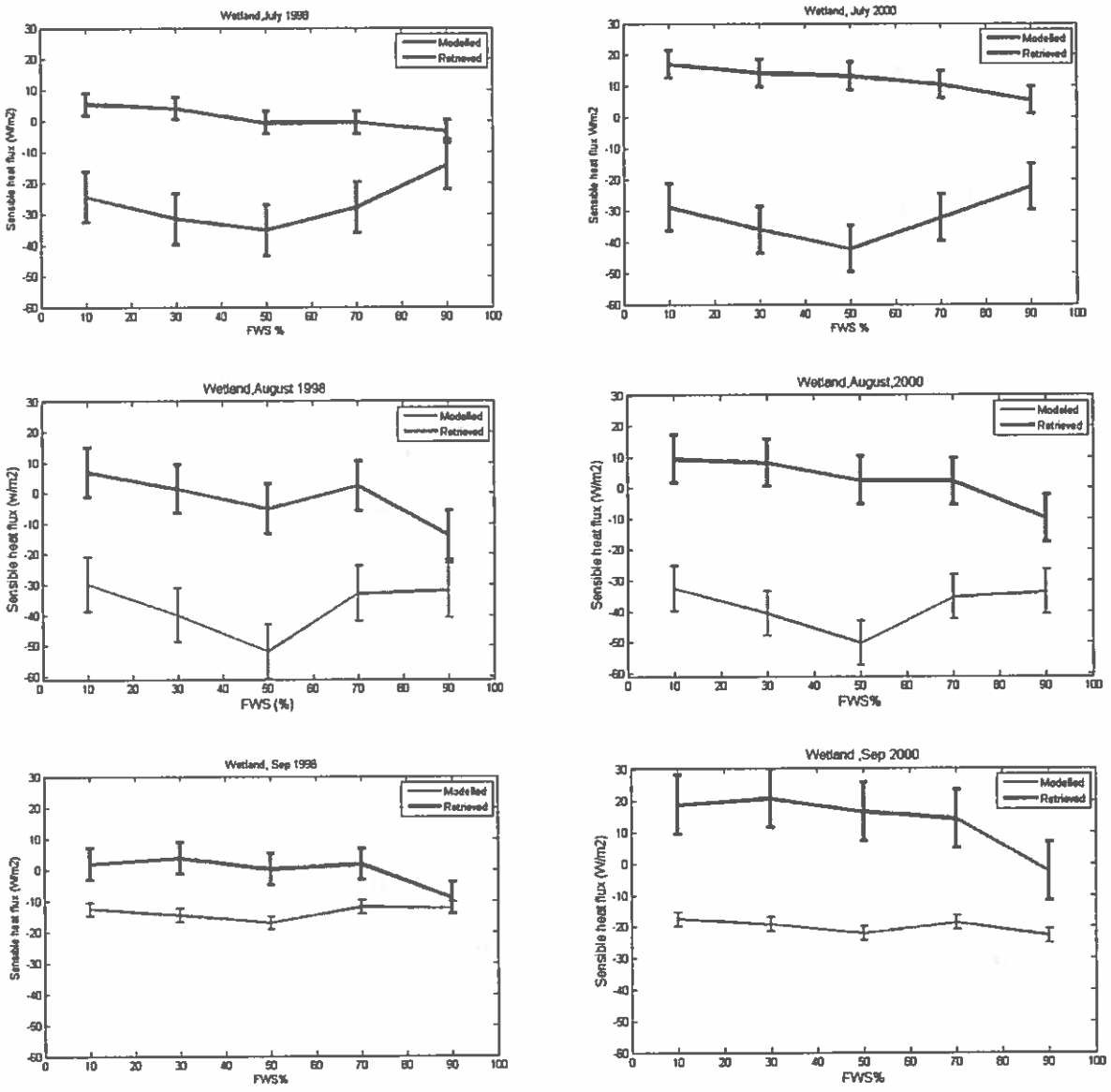

Figure 15. Average sensible heat flux versus FWS*%, Wetland

*The length of the vertical bars indicates twice the standard deviation for each interval.

It should be noted that for Wetland site, there are less variations of sensible heat flux versus FWS in comparison with the GSL site in the same period. Not only the retrieved results but also the modelled results show this pattern.

6.2 Importance of lake size

In order to study the degree of importance of lake size in the variation of the sensible heat flux, we considered cases with less than 20% FWS as a "No FWS" (NF), from 30-50% FWS as a "Small FWS" (SF), from 50-80% FWS as a "Medium FWS" (MF), and from 80-100% as a "Large FWS" (LF).

The daily average flux of sensible heat over these classes of fraction of water surface was estimated from retrievals and the NARR model. Figure 16 shows the daily values of retrieved (right hand) and modelled (left hand) sensible heat flux for three different classes, SF, MF and LF. As Figure 16 shows, the modelled sensible heat flux for the SF and MF are either very close or the same. However, for the retrieved flux, there are relatively more discrepancies between SF and MF classes.

In order to quantify these discrepancies, we used the Mean Absolute Error (MAE) as sensible heat flux measure difference between small FWS (SF) and medium FWS (MF).

$$MAE = \frac{1}{N_{total}} \sum_{i=1}^{total} \left| SHF_i - SHF_i^* \right| \qquad (24)$$

where SHF_i and SHF_i^* are the daily mean sensible heat flux values for the small FWS and medium FWS (MF) respectively. N_{total} is the total number of days involved in the MAE. The derived MAE values are given in Table 4. The comparison of the retrieved MAE with the modeled MAE shows less sensibility of the model for small FWS and medium FWS.

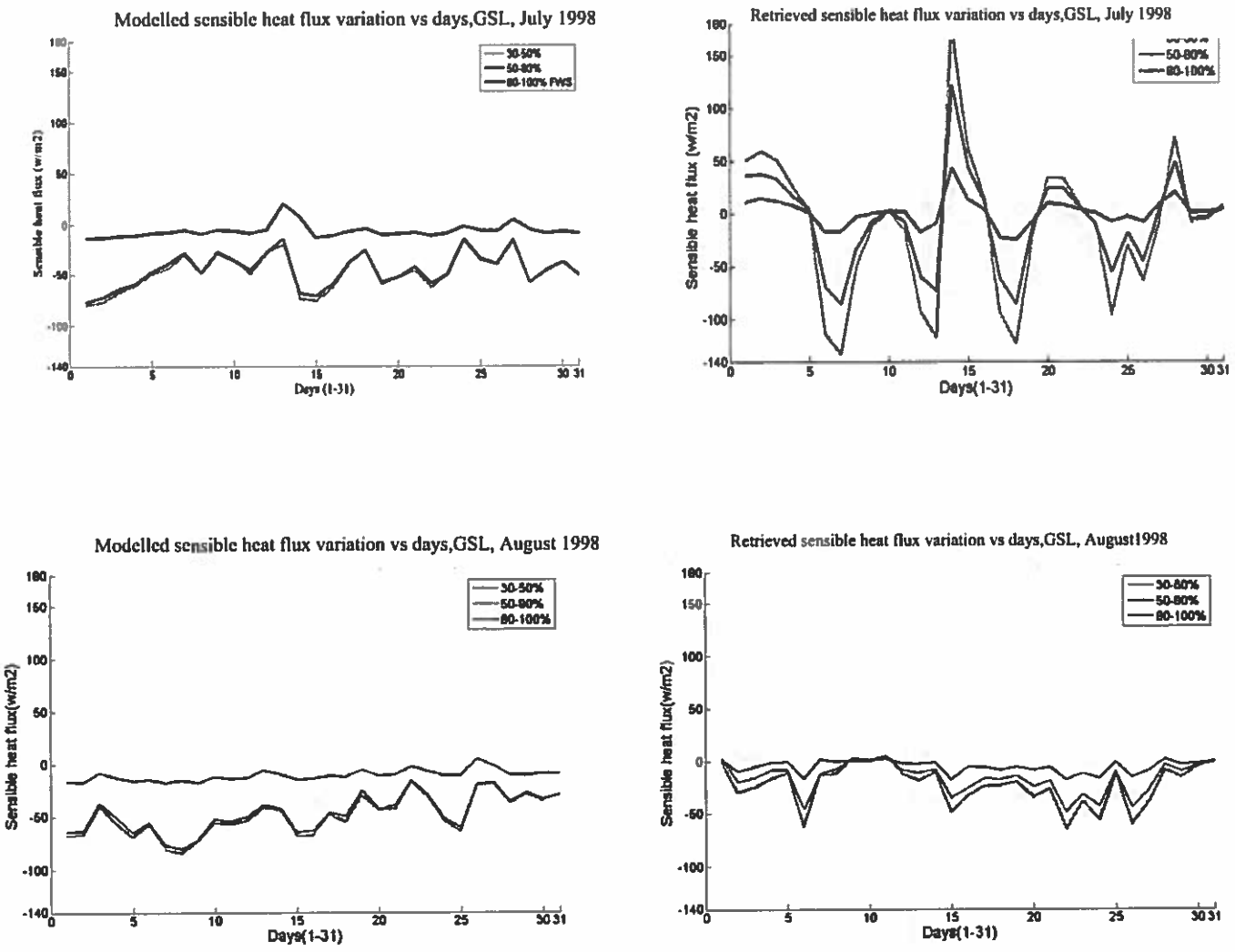

Figure 16. Daily values of sensible heat flux for GSL site for SL, ML and LL classes separately, July and August 1998*

*The retrieved data are shown in the left and the modelled in the right hand.

Table 4. The MAE values (absolute difference between small and medium FWS) for modelled and retrieved heat flux over July and August 1998

Result	MAE (July 1998)	MAE (August 1998)
Model	5.59	8.65
Retrieved	17.91	12.56

6.3 Seasonal (monthly) sensible heat fluxes variation

In this part, surface-air temperature gradient (T_s-T_a) and monthly mean values of sensible heat fluxes versus FWS for the study sites were retrieved. Figures 17, 18, 19, and 20 show the surface-air temperature gradient and monthly sensible heat flux variations for GSL and Tundra. As mentioned before for the GSL site in 2000, because of the snow cover, the month of June is incomplete. For the same reason, the graphs start with the month of July for the Tundra site.

For the GSL and Tundra sites with an increasing FWS, surface-air temperature gradient and sensible heat flux magnitude typically decreases. In accordance with the increasing (decreasing) magnitude of surface-air temperature gradient, the partition of net radiation into sensible flux increased (decreased). Furthermore, we can say that when the FWS approaches 80-100%, the sensible heat values of the different months tend to overlap. Alternatively, when the FWS is small (1-20%), the sensible heat values of different months are much more dispersed.

In general, at GSL (forested area), sensible heat decreases significantly from 40-60 W/m^2 to 0-10 W/m^2. Over Tundra, the decreasing trend is less marked, from -20 W/m^2 to 0 W/m^2 (except for the month of September 2000 where a significant increase is observed from -100 W/m^2 to -10 W/m^2).

Figures 21, 22, 23 and 24 show the patterns differ for the Wetland and Taiga sites. For the Wetland site, there is reverse variation; sensible heat is positive (+20/+10 W/m^2) for FWS<20%, and sensible heat flux varies between +10 and -10 W/m^2 depending on the month. For the Taiga site, sensible heat flux is relatively constant when the FWS rises.

The year 2000 is representative of a normal summer, while the year 1998 was very warm (the warmest summer of the century). Both years, 1998 and 2000, show steeper surface-air temperature gradients and larger sensible heat flux magnitude for the month of September, and the year 2000 presents the largest values for these two years.

Temperature gradient trends are different for 1998 and 2000. A warmer summer (1998, El Nino year) presents a smaller surface-air temperature gradient than summer 2000,

For the year 1998 in general, the seasonal heat flux for June and July is always lower (0-20 W/m2) than the end of the season (August and September), except for the Taiga site, where seasonally is not apparent.

Therefore, the observed variations of sensible heat versus the FWS depend on the land cover types surrounding the lakes, the summer months and the year considered.

As Figure 24 shows, there are inconsistencies in the results between the Taiga site and the other sites, especially in the year 2000. For example, in 2000, the error bars for intervals 1-20% and 21-40% FWS show very close overlaps. On the other hand, for the intervals 61-80% and 81-100%, there is less overlap. In 1998 the mean values versus the FWS are very close (see the mean values for intervals 1-20% and 80-100%). In section 6.4 we discuss more about the Taiga site.

In most cases, there are decreases in sensible heat with increasing FWS (except for the Taiga site). As a result, the inclusion of bodies of water in the underlying surface decreases the sensible heat flux.

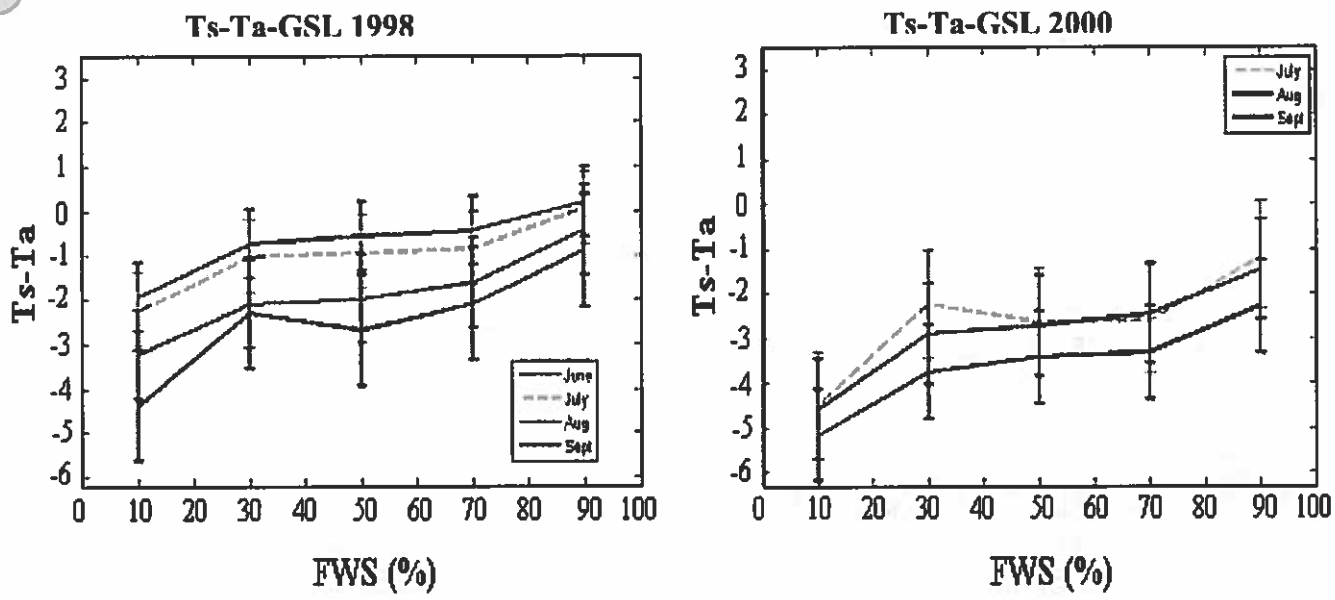

Figure 17. Average surface-air temperature gradient versus FWS% for four months (June, July, August, and September) in 1998 and 2000 for the GSL site

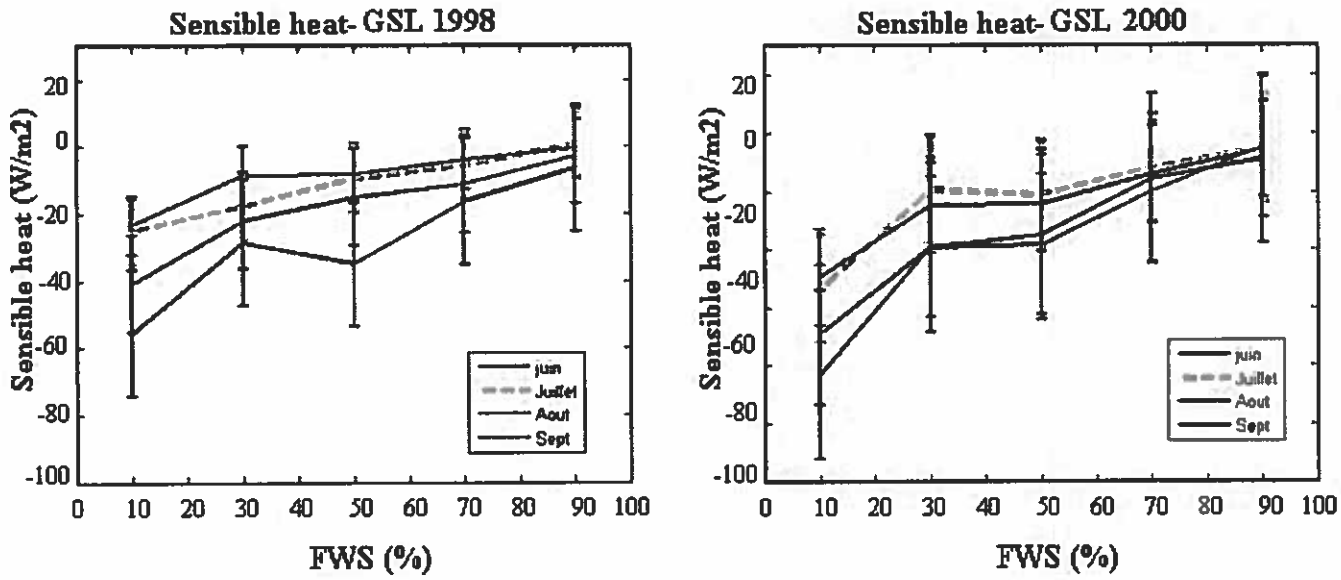

Figure 18. Average sensible heat fluxes (retrieved) versus FWS% for four months (June, July, August, and September) in 1998 and 2000 for the GSL site

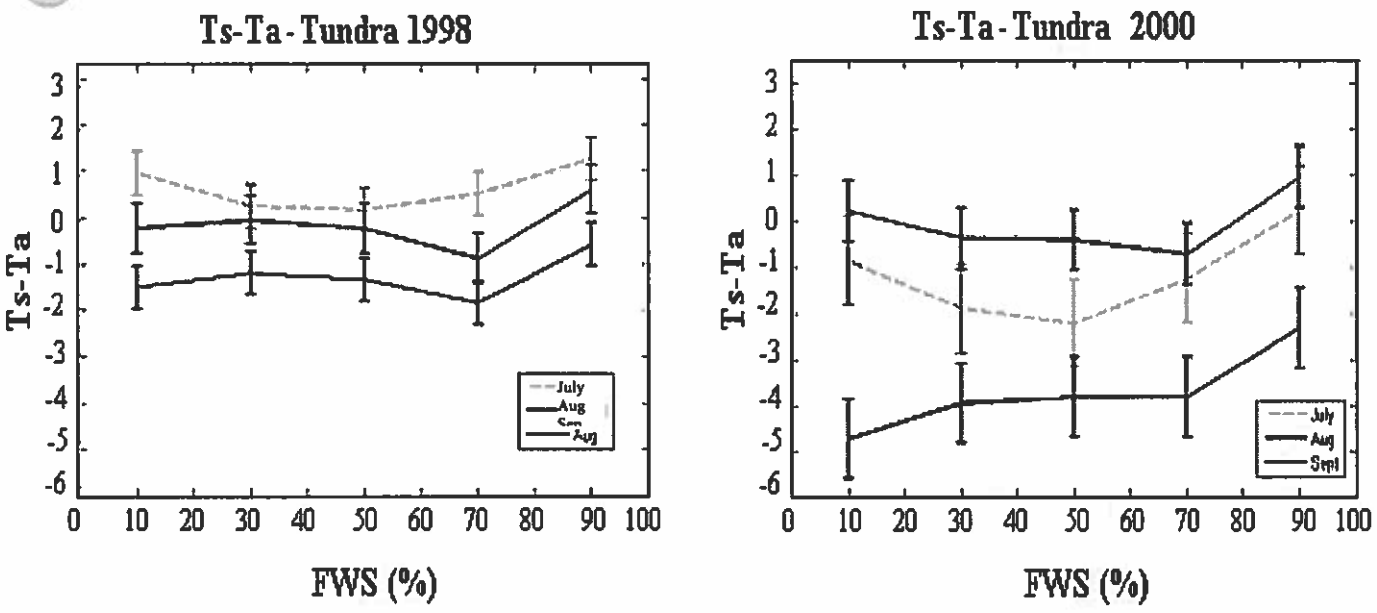

Figure 19. Average surface-air temperature gradient versus FWS% for three months (July, August and September) in 1998 and 2000 for the Tundra

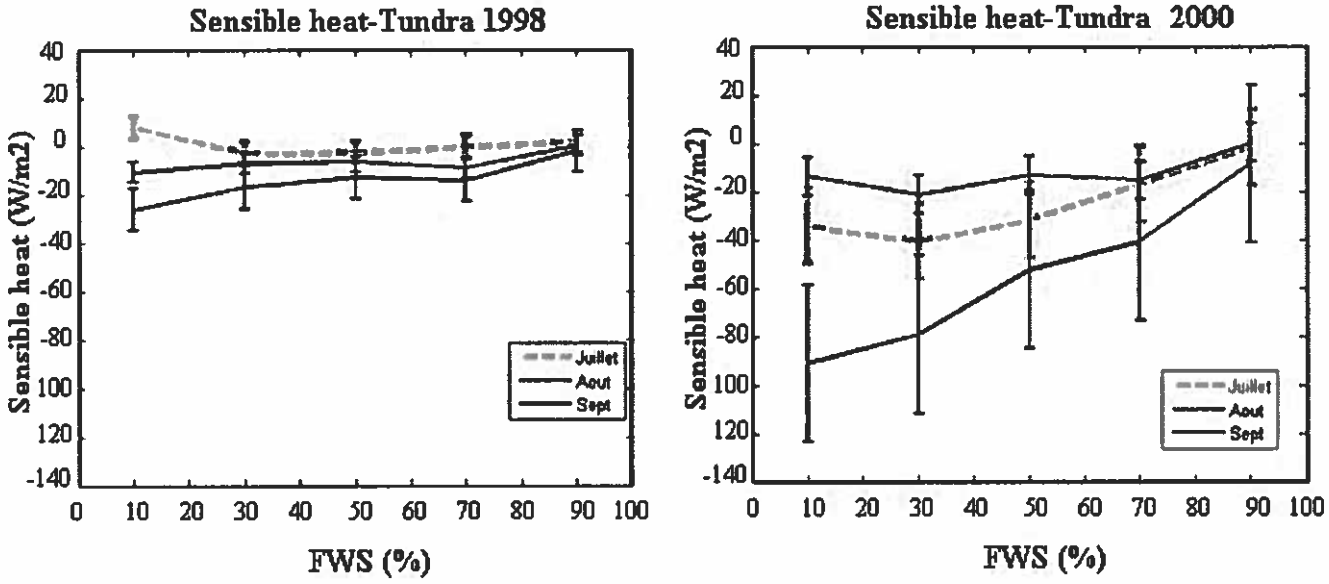

Figure 20. Average sensible heat fluxes (retrieved) versus FWS% for three months (July, August and September) in 1998 and 2000 for the Tundra

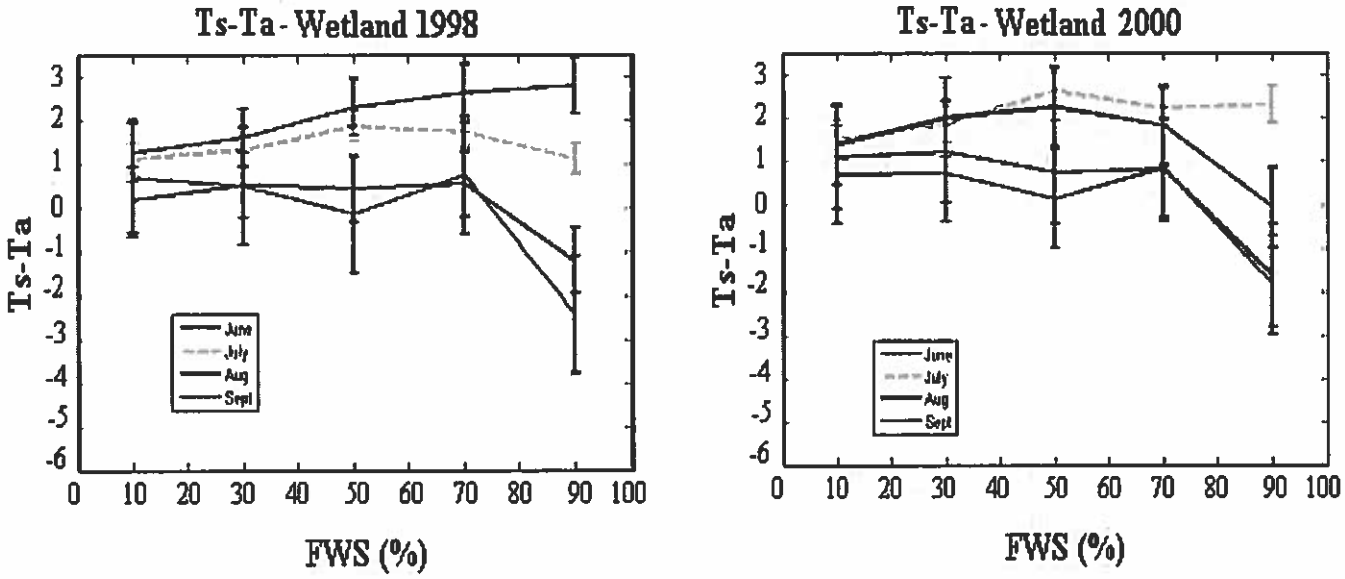

Figure 21. Average surface-air temperature gradient versus FWS% for four months (June, July, August, and September) in 1998 and 2000 for the Wetland site

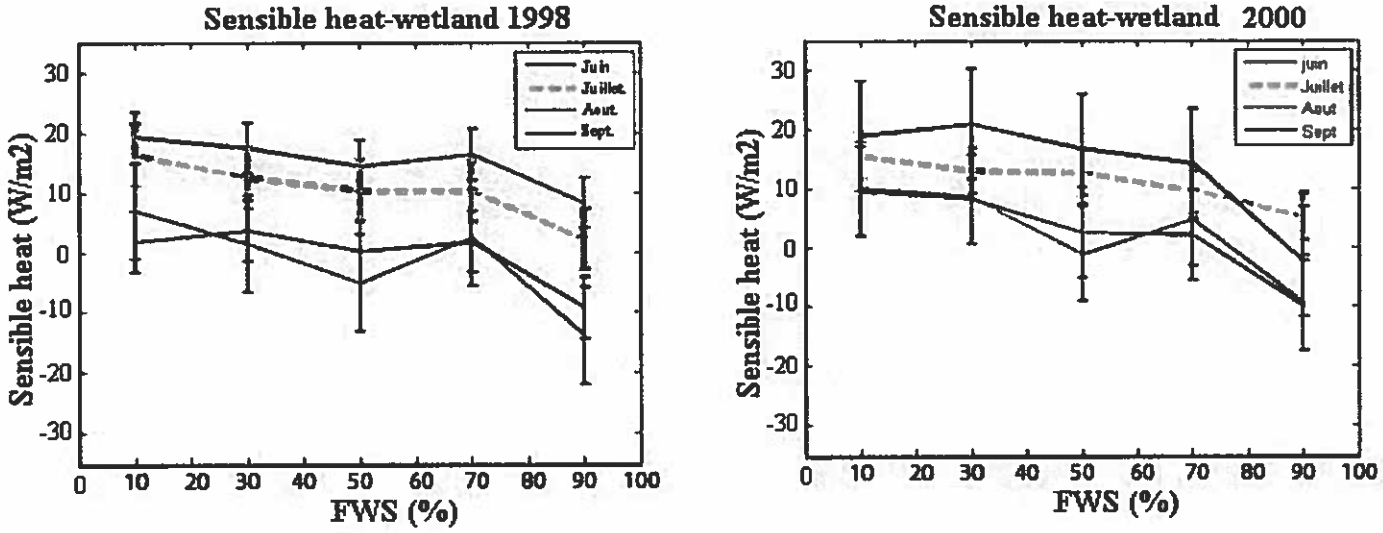

Figure 22. Average sensible heat fluxes (retrieved) versus FWS% for four months (June, July, August, and September) in 1998 and 2000 for the Wetland site

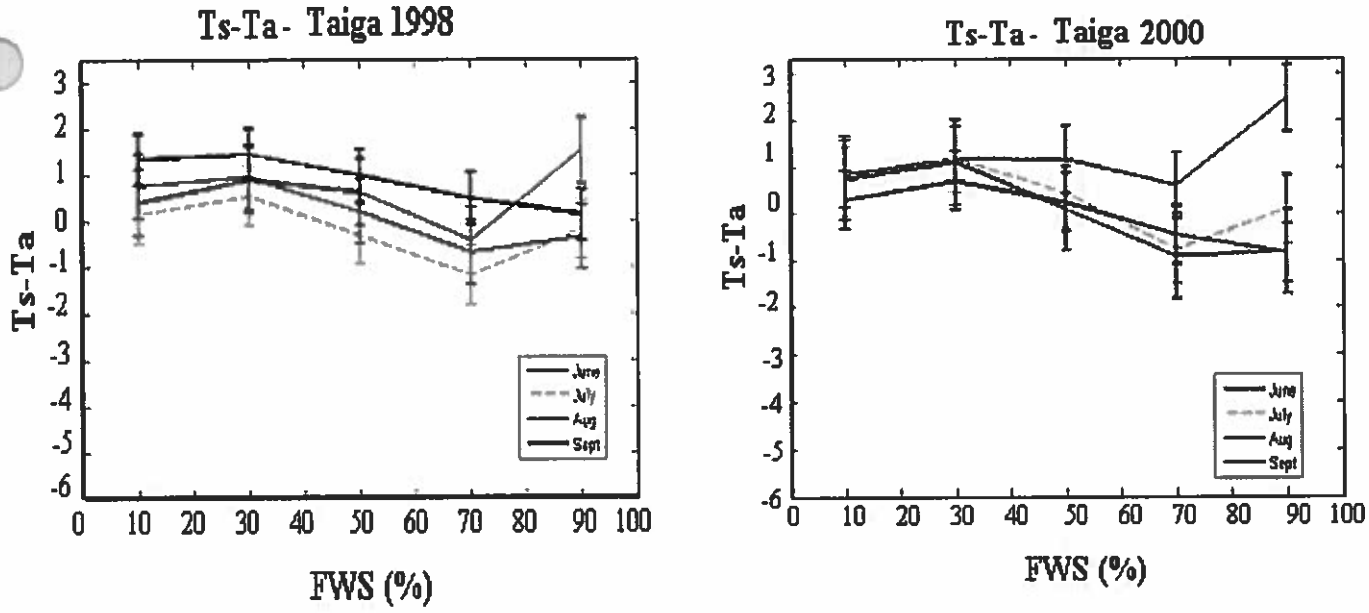

Figure 23. Average surface-air temperature gradient versus FWS% for four months (June, July, August, and September) in 1998 and 2000 for the Taiga site

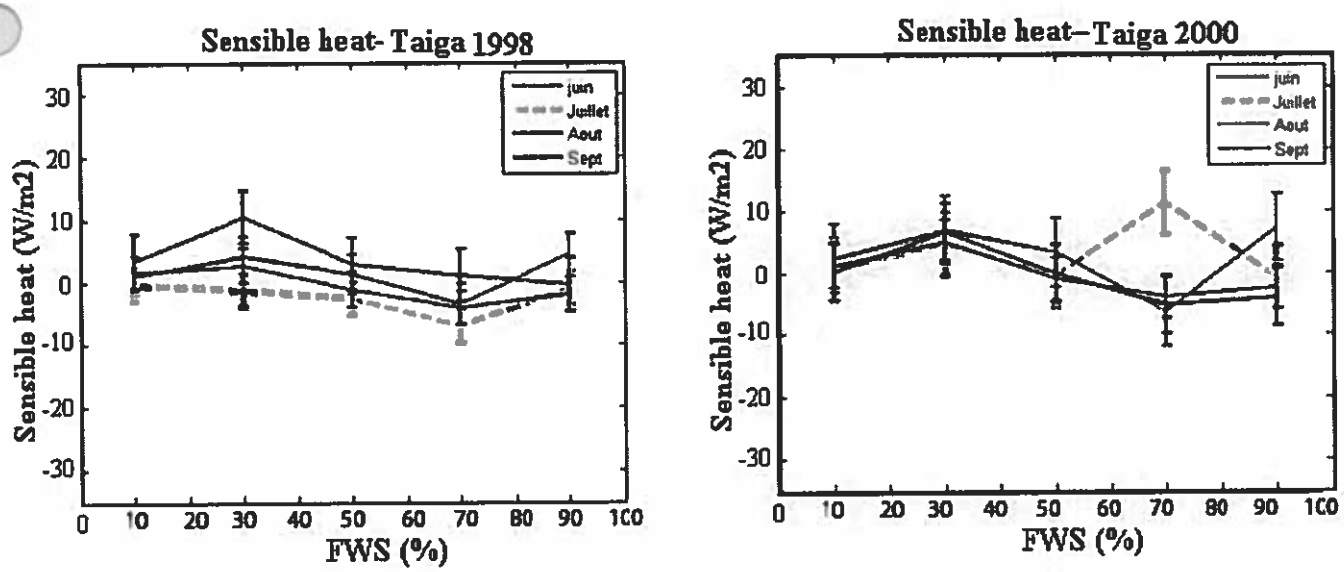

Figure 24. Average sensible heat fluxes (retrieved) versus FWS% for four months (June, July, August, and September) in 1998 and 2000 for the Taiga site

To better understand the spatial-temporal sensible heat variation, the energy balance relationships for the previously mentioned categories of FWS and for two different time intervals were calculated. The two time intervals were defined as follows:

1- First half of the summer: Early season (June 10 to July 20).
2- Second half of the summer: Late season (July 21 to August 30).

The (y/x) ratio was calculated for the two time intervals. The parameter x specifies the sensible energy balance component when there is less than 20% FWS (No FWS) and y is the sensible heat flux for the three different FWS classes (SF, MF, LF). This approach allows us to normalize each site by their respective reference without lake that renders possibility the comparison between sites, having their own climate condition.

In order to determine the effect of different land type on sensible heat flux partition, the estimated and modelled ratios (y/x) are considered for 4 different sites. The early and late season periods have been distinguished. Figure 25 shows the ratio (y/x) for the GLS, Wetland, Taiga, and Tundra sites in 1998 and Figure 26 shows the ratio for 2000. The values of ratio are given for each site separately: Table 5. GSL; Table 6. Wetland; Table 7. Taiga; and Table 8. Tundra.

Figures 25 and 26 show the maximum retrieved ratios for the Taiga and Tundra sites and the minimum retrieved values for the GSL and Wetland sites. Such different results are mainly derived from the sites' different land cover types. The predominant terrain type for the Tundra and Taiga sites is open tundra with less vegetation. This means that in these areas the greater part of the net radiant energy has to be converted into sensible heat and ground heat fluxes. Therefore, Figures 25 and 26 imply that the effects of lakes are closely related to the local setting of the lake and its surroundings. This is due to the difference in heat capacity, roughness length of water compared with nearby forest. In addition, Figures 25 and 26, just like the preceding results, show modelled ratios changed very little from one class of FWS to another, and suggests that the model is insensitive to the FWS in the interval 30-80%. Some examples are highlighted in green in Tables 5, 6, 7, and 8.

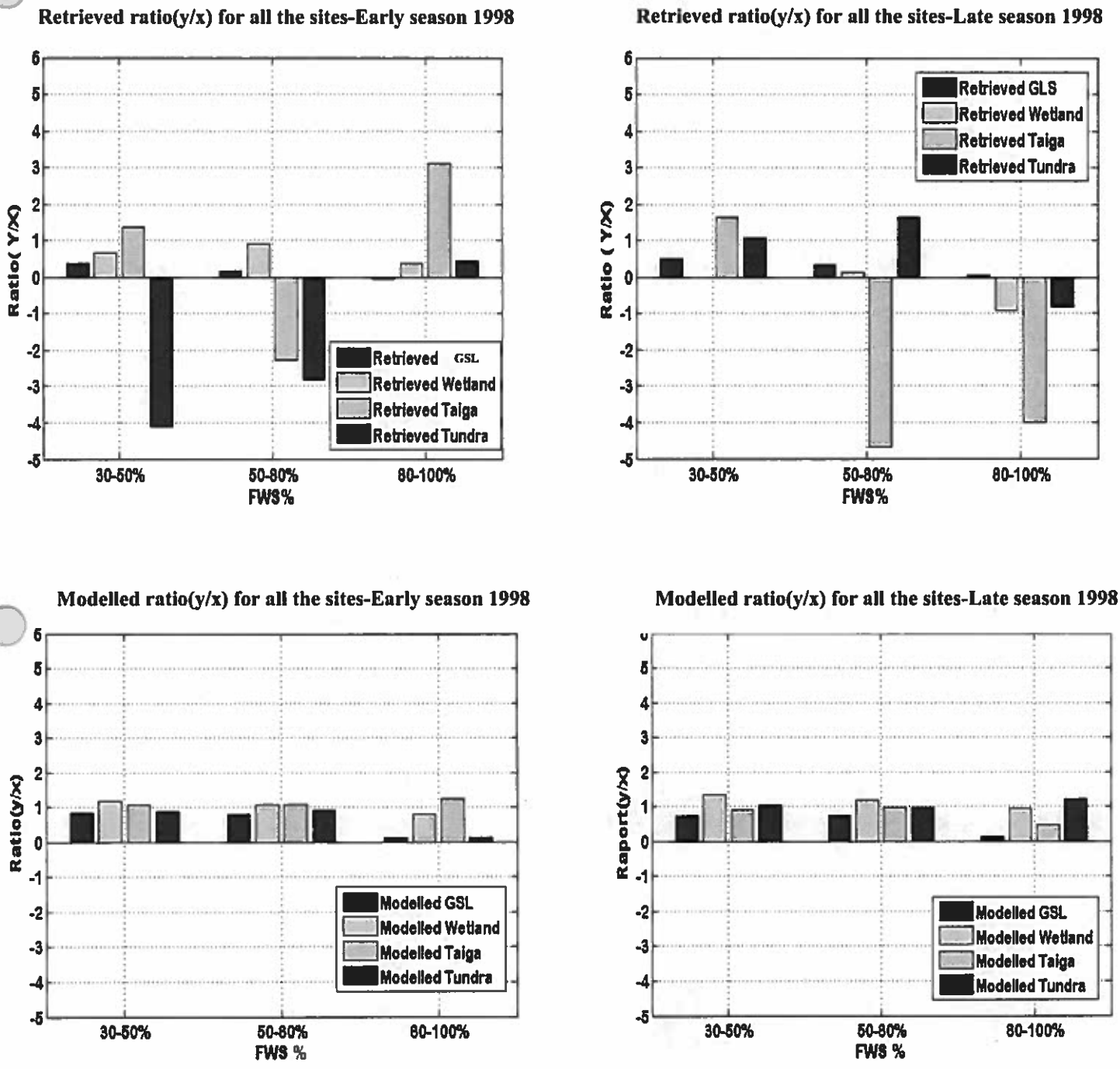

Figure 25. Comparison of the 4 sites - modelled and retrieved values over the summer of 1998

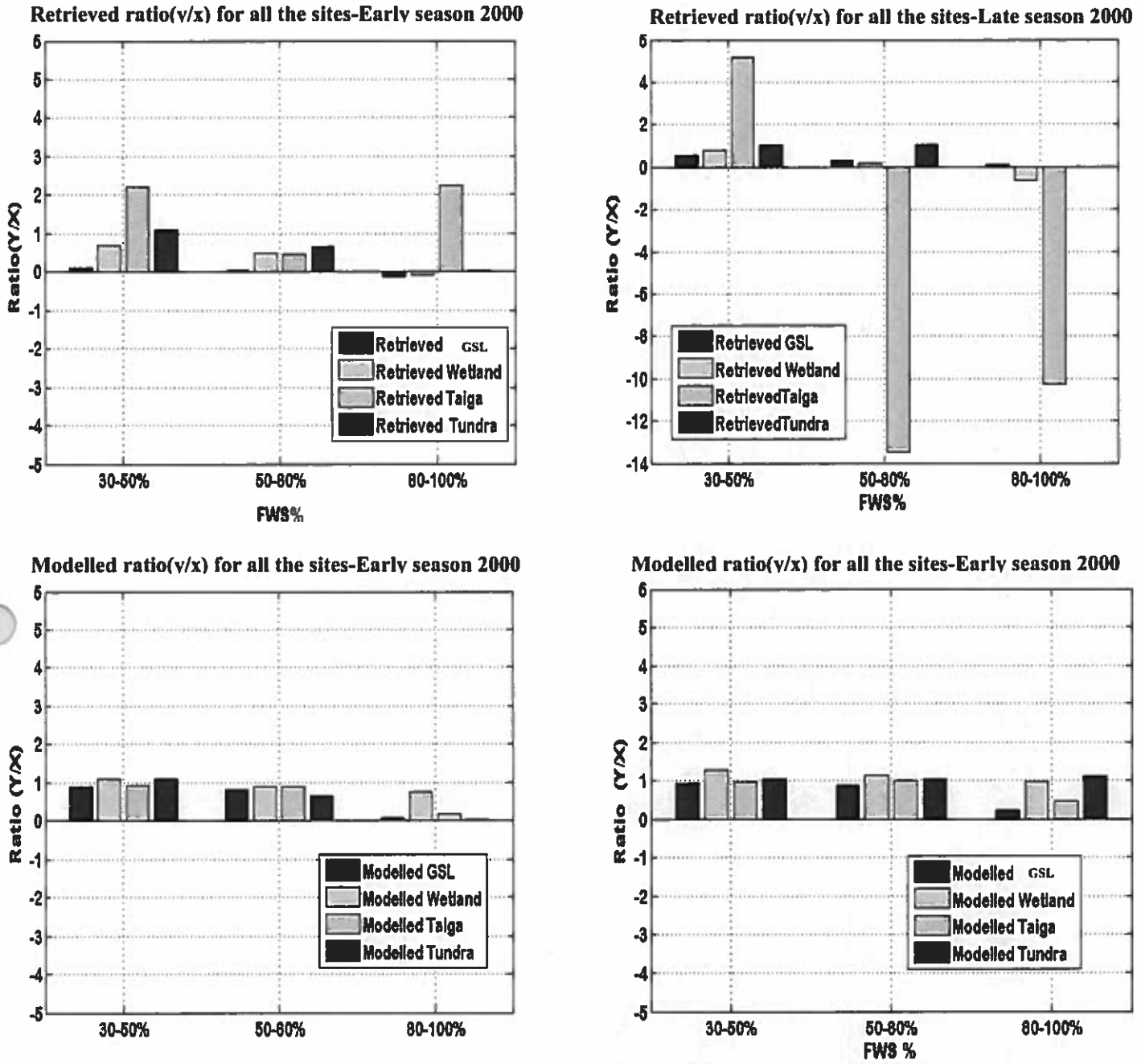

Figure 26. Comparison of the 4 sites - modelled and retrieved values over the summer of 2000

For the GSL site, for example, the modelled ratio (y/x) computations change little from the SF to MF classes; 5% and 8% for early 1998 and 2000 respectively, and 1% and 6% for late 1998 and 2000 respectively. Regarding the retrieved ratio, the variation is greater, for example 54% and 63% for early 1998 and 2000 respectively, and 37% and 49% for late 1998 and 2000 respectively(Appendix 4). Table 6 shows that for the Tundra (2000) the modelled values for the two different classes, SF and MF, are the same. http://dictionnaire.reverso.net/anglais-francais/well-known

As a result, for the SF and MF classes, the more available energy is converted into sensible heat, while the retrieved results (which are based on considering carefully fraction of surface water) show less energy converted into sensible heat. There are approximately the same patterns for the other sites.

A comparison of the Early Season and Late Season indicates that for the GSL, Tundra and Taiga sites, the sensible heat flux values are more important during the Late Season. However, it is different for the Wetland site.

It should be noted that based on the results of Figures 25 and 26, the ratio of the Taiga site is very high compared to the others. Therefore, we have doubts concerning the ratio (y/x) for the Taiga site (similar to the results in Figure 24). Thus, the forcing data were controlled and we determined the source of the error. The error in the retrieved sensible heat is introduced by remotely sensed Ts.

However, the reason for such uncertainly needs to be investigated with the help of field datasets or in situ measurements. Therefore, the accurate calculation of sensible heat flux requires ascertaining the data. Any error in the forcing data propagates through retrieved algorithm and affects the final estimates.

Table 4. Ratios (*y/x*) for the GSL site

Site	GSL					
Period	Early Season			Late Season		
class	SF	MF	LF	SF	MF	LF
Retrieved 1998	0.35	0.16	-0.02	0.51	0.32	0.06
Retrieved 2000	0.11	0.040	-0.14	0.51	0.26	0.10
Modelled 1998	0.85	0.80	-0.13	0.75	0.74	0.17
Modelled 2000	0.89	0.81	0.08	0.93	0.87	0.22

Table 5. Ratios (*y/x*) for the Wetland site

Site	Wetland					
Period	Early Season			Late Season		
class	SF	MF	LF	SF	MF	LF
Retrieved 1998	0.66	0.91	0.36	0.01	0.12	-0.90
Retrieved 2000	0.67	0.50	-0.08	0.78	0.19	-0.65
Modelled 1998	1.10	1.00	0.81	1.30	1.10	0.93
Modelled 2000	1.10	0.90	0.74	1.30	1.10	0.97

Table 6. Ratios (*y/x*) for the Taiga site

Site	Tundra					
Period	Early Season			Late Season		
class	SF	MF	LF	SF	MF	LF
Retrieved 1998	-4.10	-2.80	0.44	1.10	1.70	-0.82
Retrieved 2000	1.10	0.66	0.50	1.00	1.00	0.01
Modelled 1998	0.88	0.90	0.11	1.00	0.98	1.90
Modelled 2000	1.10	0.70	0.15	1.00	1.00	1.10

Table 7. Ratios (*y/x*) for the Tundra site

Site	Taiga					
Period	Early Season			Late Season		
class	SF	MF	LF	SF	MF	LF
Retrieved 1998	1.39	-2.30	3.10	1.60	-4.60	-4.60
Retrieved 2000	2.20	0.43	2.20	5.20	-13.8	-10.30
Modelled 1998	1.00	1.10	1.30	0.92	0.97	0.46
Modelled 2000	0.91	0.90	0.16	0.96	1.00	0.47

6.5 Comparison of 1998 and 2000

For different sites, we retrieved the ratio(y/x) for the summer months of 1998 and 2000. Then we showed the ratio for the three classes separately. Therefore, there are three images for three LF, MF and LF classes which consider all the study sites.

As Figures 27 and 28 shows, the differences between 1998 and 2000 are minimal for Wetland site. This indicates that the different temperature condition has less effect on the energy balance of the Wetland site in comparison with the other sites. The surface energy of the Wetland site is thus more strongly influenced by its terrain than by climatic differences.

About the LF class, Figure 29 illustrates that there are minimum annual variations for GSL, the site which is covered mostly by water (Great Slave Lake).

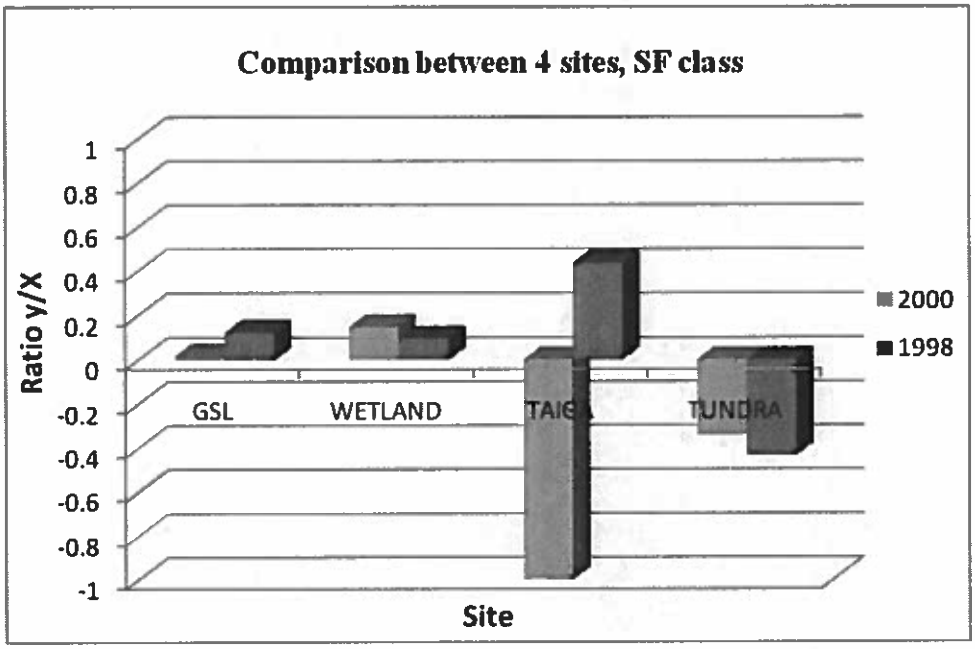

Figure 27. Comparison (y/x) ratio of 4 sites over 1998 and 2000, SF class

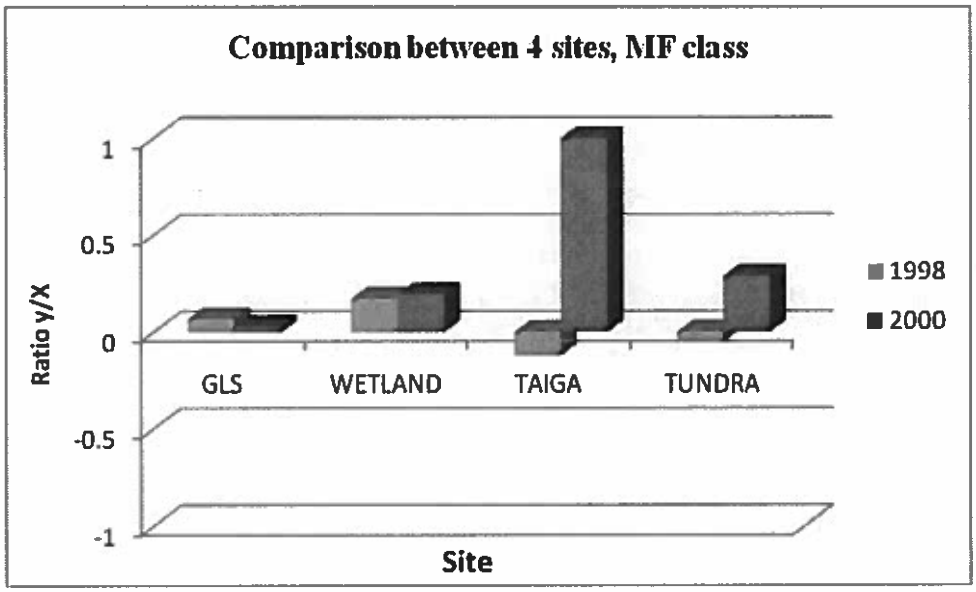

Figure 28. Comparison (y/x) ratio of 4 sites over 1998 and 2000, MF class

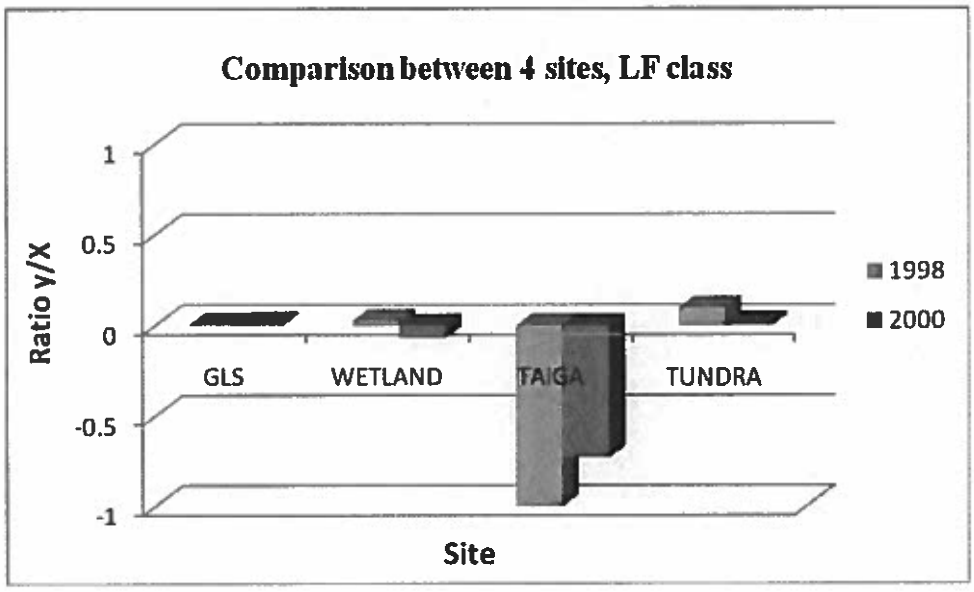

Figure 29. Comparison (y/x) ratio of 4 sites over 1998 and 2000, LF class

6.6 Bowen ratio estimation – GSL and Wetland sites

The Bowen ratio results for the GSL and Wetland sites are presented in this section. The higher absolute value of β ($\beta > 1$) indicates the dominance of sensible heat. On the other hand, the lower absolute value of β ($\beta < 1$) is an indication of the dominant latent heat (Castellvi, 2006).

These ratios are retrieved for two different sites, GSL and Wetland over two periods: early and late summer as a function of the FWS. The values of the Bowen ratio for the GSL and Wetland sites are given in Tables 8 and 9 respectively. For both sites, the available energy is mainly under the form of latent heat (the maximum absolute value of the ratios is less than 0.36).

Figure 30 shows that the magnitude of the Bowen ratios for GSL tends to decrease with increasing water contents. The greater presence of FWS enhances evaporation and thereby increases the contribution of latent flux and decreases the sensible heat flux. This leads to a reduction in the value of the Bowen ratio with increasing FWS.

Comparing Bowen ratios between the early and late periods shows an increase of β for the late period for GSL (this supports the second hypothesis), and this trend is similar for both 1998 and 2000. The increasing Bowen ratio can be interpreted as an indicator of increasing water stress over the late summer period.

Figure 31 shows the magnitude of the Bowen ratio for the Wetland site. For the Wetland site, there is no clear difference between the two periods, Early and Late. According to Table 9 and Figure 31, there is very little difference between the two periods, Early and Late, as well as between the two different years, 1998 and 2000.

However, it should be noted that for the GSL site, the magnitude of the Bowen ratio values are a little greater in 2000 than for the corresponding period in 1998 (marginally so in the Wetland case).

A comparison of the two sites over the two years indicates that the GSL site was more sensitive to temperature variation (warm year 1998, cold year 2000) than the Wetland site. Therefore, the change in the Bowen ratio is not only caused by "atmospheric condition" but also by the "land cover."

Table 8. Bowen ratio values for GSL site

Period	Early Season - GSL				Late Season - GSL			
Class	NF	SF	MF	LF	NF	SF	MF	LF
1998	-0.11	-0.06	0.04	0.01	-0.29	-0.18	-0.13	-0.02
2000	-0.29	-0.19	-0.13	-0.03	-0.35	-0.25	-0.18	-0.06

Table 9. Bowen ratio values for Wetland site

Period	Early Season - Wetland				Late Season - Wetland			
Class	NF	SF	MF	LF	NF	SF	MF	LF
1998	0.20	0.11	0.12	0.05	0.17	0.06	-0.01	-0.09
2000	0.16	0.10	0.12	0.06	0.16	0.12	0.05	-0.07

6.7 Comparisons with in situ measurements

Comparing the retrieved results with in situ measurements was not an easy task. The ideal situation would be for energy to be measured simultaneously at the retrieval period, which is not always possible. For this reason there is no comparable data for the Wetland site. Furthermore, the results obtained from in situ measurements are limited in areal extent and represent an unequal areal as compared with those from retrieval algorithms.

The modelled and retrieved results are compared with the results of in situ measurements by Rouse et al. (2001) over the period spanning June 15 to August 31 for the different years. In order to achieve a quantitative comparison, we present a set of 8 maps of the spatial distribution of sensible heat fraction (H/R_{net}) for the GSL and Wetland sites (Figures 32 and 33).

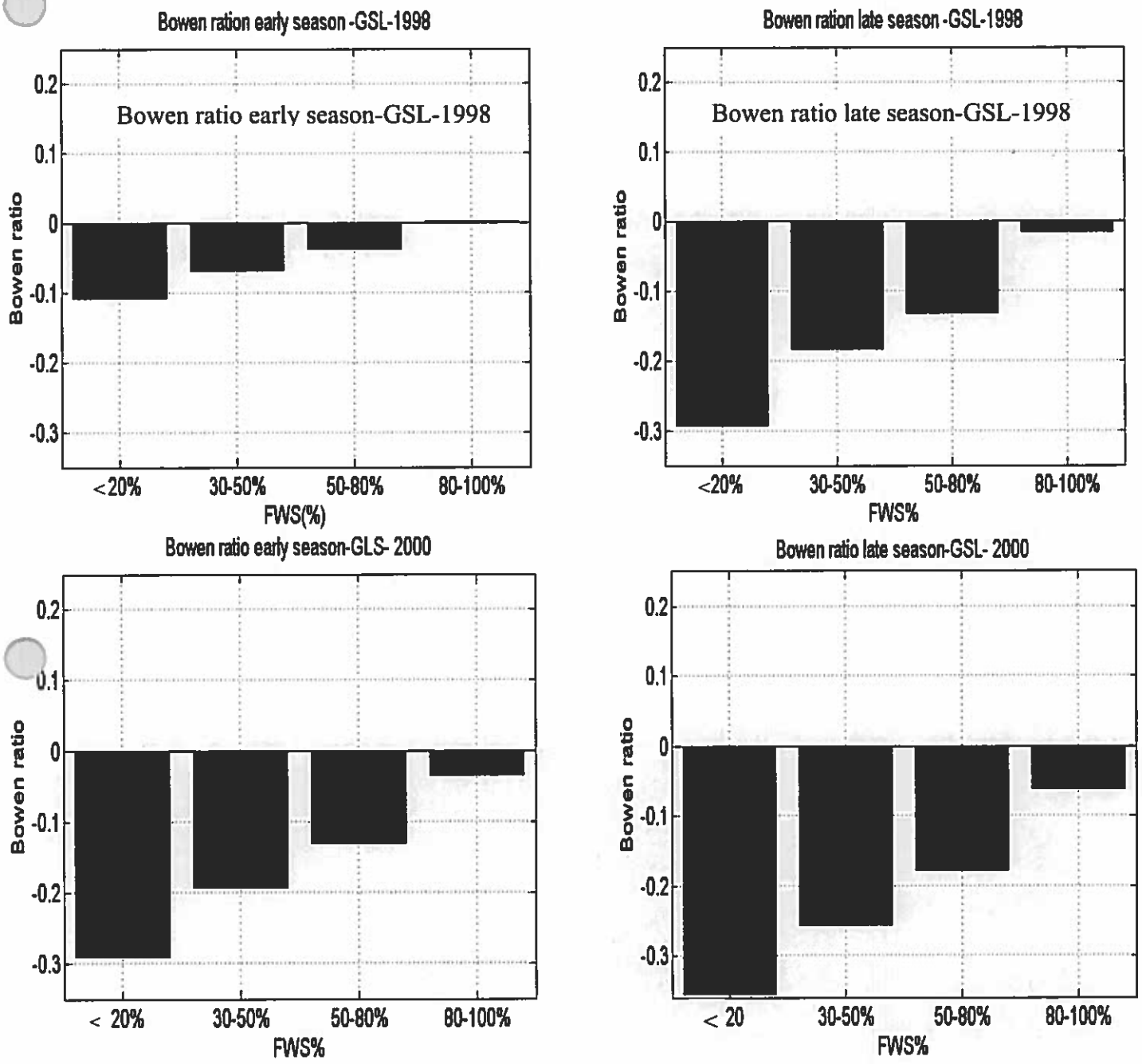

Figure 30. Bowen ratio as a function of FWS% for the GSL site – years 1998 and 2000

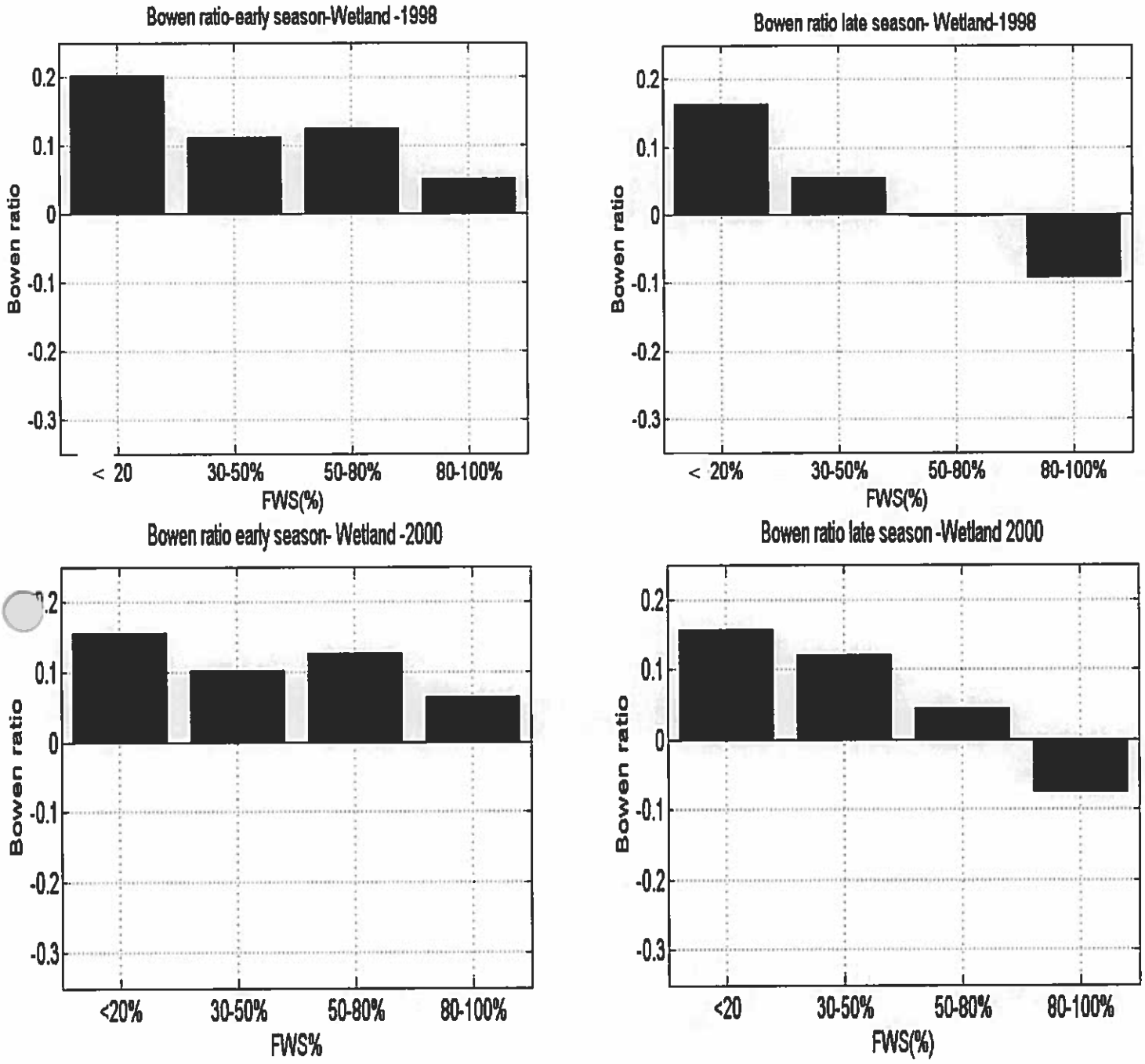

Figure 31. Bowen ratio as a function of FWS% for the Wetland site – years 1998 and 2000

1998 and 2000 at a spatial resolution of 25km*25km.The EASE-GRID projection was prepared for retrieved and modelled results. There were two research sites. The first one was located near the main body of Great Slave Lake, on a rock islet known as Inner Whaleback Island.

Table 10 makes it possible to compare in situ measured values with modelled and retrieved values. It should be noted that there are only two in situ measurements over the summers of 1997 and 1998. As Table 10 indicates, the retrieved results for GSL (1998) are closer to in situ results compared to the modelled one.

Table 10. Comparison of H/R_{net} ratio with in situ (Rouse et al., 2001) – GSL

Results / Year	Rouse	Retrieved	Modelled
1997 (normal)	0.04	-	-
1998 (warm)	-0.06	-0.08	0.01
2000 (cold)	-	0.01	0.02

The second comparison is for the Wetland site. In situ measurements were acquired 18 km southeast of Churchill, Manitoba, over the summers of 1990 to 1995 (June 15 to August 31). It should be noted that there are no overlapping years between the retrieved and the in situ results. Figure 33 shows the spatial distribution of the (H/R_{net}) ratio for the same period.

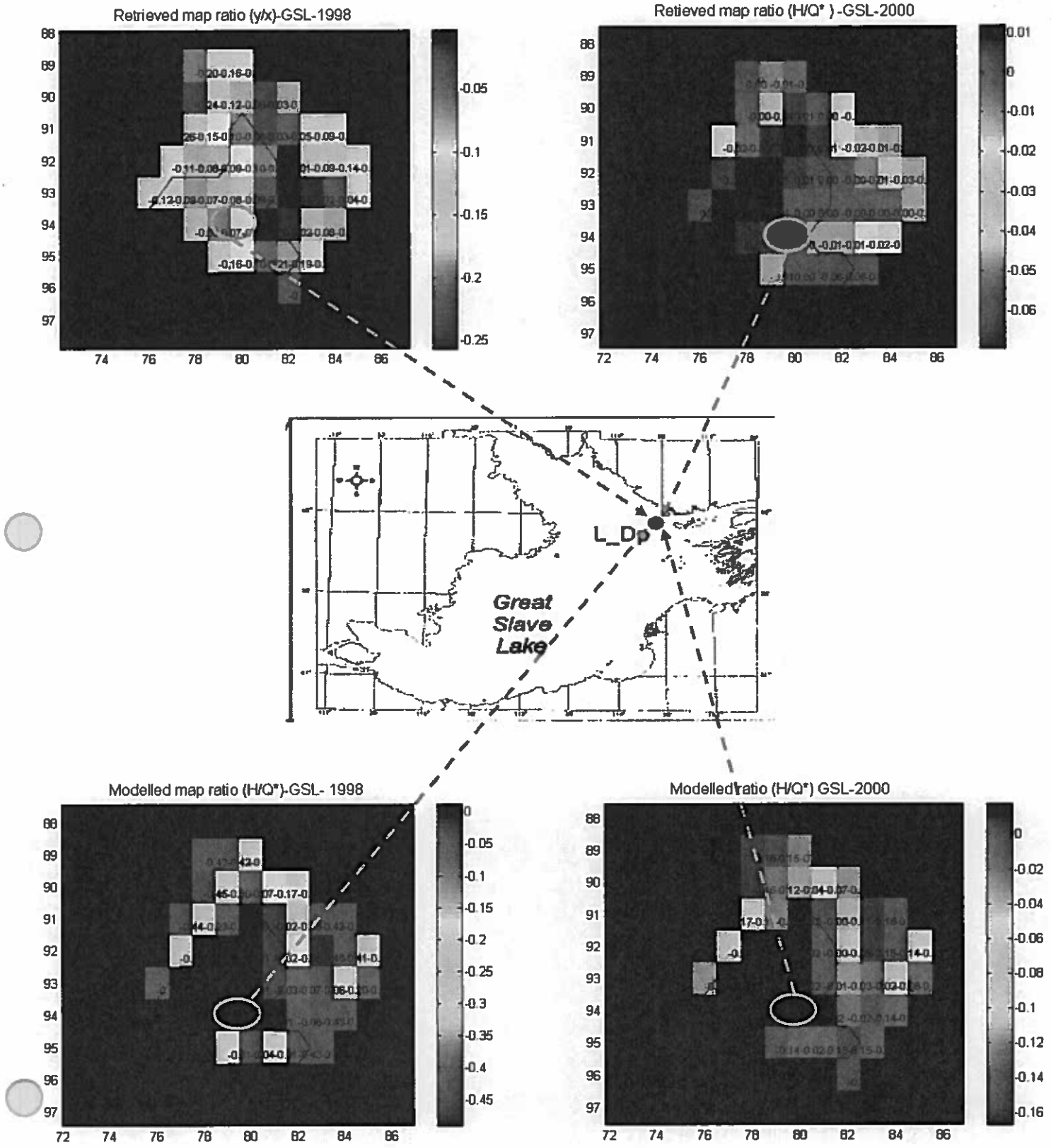

Figure 32. Spatial distribution of the H/R_{net} ratio for the GSL site, modelled and retrieved

Table 11 makes it possible to compare in situ measured values with modelled and retrieved values. The ratio retrieved for the warm year of 1998 is closer to the in situ measurements (warm year of 1991) than the modelled ratio.

One of the possible reasons for the discrepancies between retrieval and in situ measurements is lake depth. The algorithm obtained does not consider the depth of lakes and there is no depth-dependent function. On the other hand, Panin et al. (2006) show that as the depth decreases, the exchange conditions increase.

Table 11. Comparison of H/R_{net} ratio with in situ (Rouse et al., 2001) - Wetland

Result / Year	Rouse	Retrieved	Modelled
1990 (moderate)	0.25	-	-
1991 (warm)	0.17	-	-
1992 (cold)	0.35	-	-
1993 (moderate)	0.3	-	-
1994 (moderate)	0.4	-	-
1995 (moderate)	0.22	-	-
1998 (warm)	-	0.09	-0.64
2000 (moderate)	-	0.08	-0.61

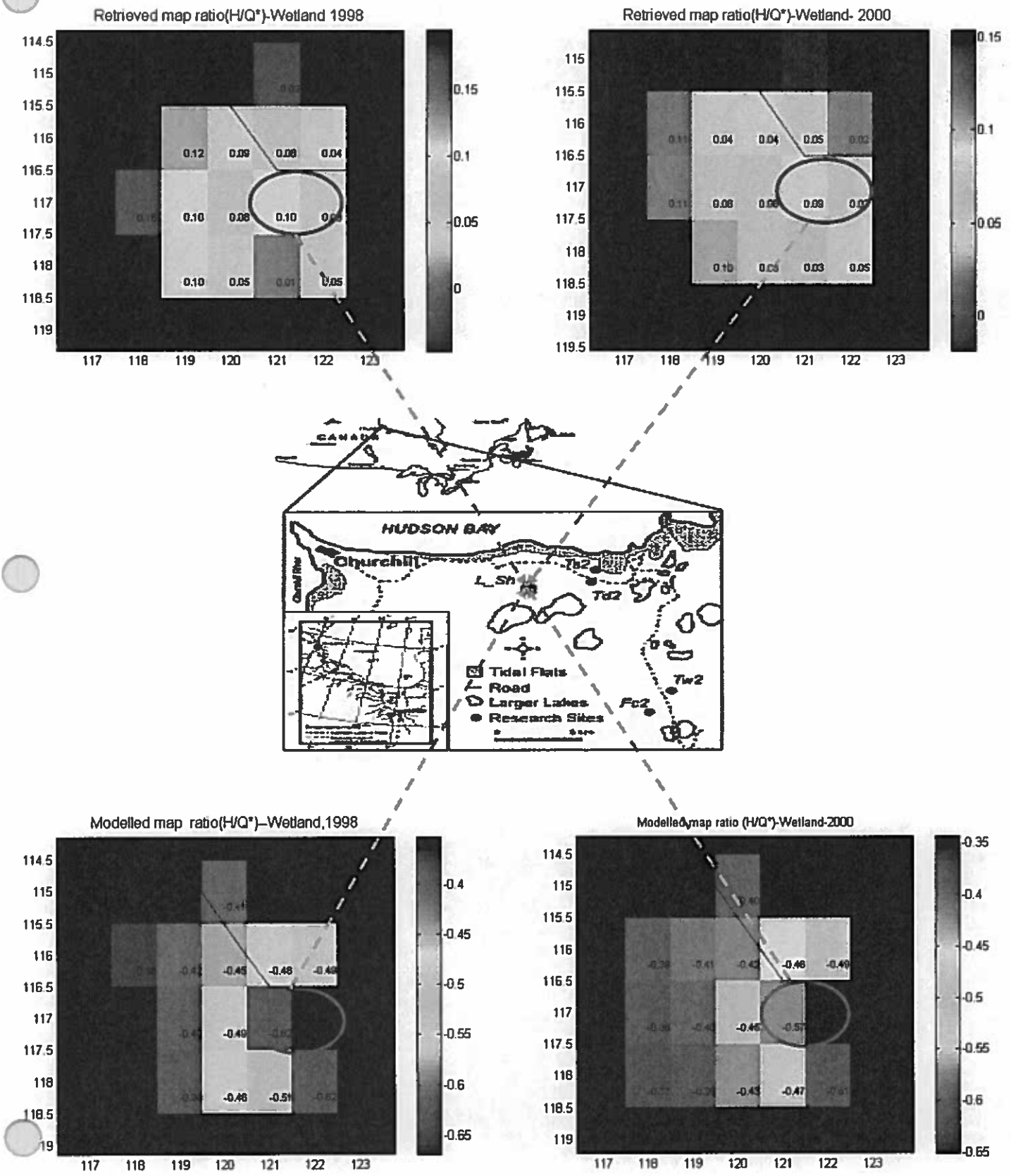

Figure 33. Spatial distribution of the H/R_{net} ratio for the Wetland* site, modelled and retrieved.
* Note that the scale of map is 5km compare to 25*25km satellite pixel.

7. Conclusion and verification of hypothesis

The results of the study show that the fraction of water surface (FWS) is important with regards to the magnitude of regional energy balance. The presence of water bodies at the surface introduces difference in surface properties that give rise to spatial variations in surface-air temperature and the partitioning of sensible and latent heat fluxes. Even if the fractional pixel area covered by water is small, the average energy flux can be different due to the presence of water. As the results indicate for the GSL and Tundra sites with the inclusion of water bodies at the surface, there is a decrease in sensible heat flux accompanied by a decrease in the surface air temperature. A comparison of the Early Season and Late Season indicates that for the GSL, Tundra and Taiga sites, the sensible heat flux values are more important during the Late Season. This conclusion supports the first hypothesis. However, the same trend does not apply to Wetlands. This is because different surface regimes lead to different energy partitioning.

The Bowen ratio results for the GSL site indicate that the NARR model is not sensitive to small and medium FWS, and this insensitivity has had a certain influence on the energy balance. The results indicate that small lakes behave differently from medium to large lakes. A comparison of the retrieved results based on the method used by Fily et al. (2003) with few in situ measurements and the NARR model show that the retrieval for some cases was closer to the in situ results.

The results for the Bowen ratio for the GSL site indicate that the ratios for the second half of the summer are greater than the first half. This conclusion supports the second hypothesis. But it should be noted that for the Wetland site, there is no a clear pattern. The results show that the energy balance of the Wetland site is more strongly influenced by its terrain than by climatic differences. We infer that the effects of the lake are closely related to the surrounding environmental conditions, such as land surface characteristics, vegetation distribution and aerodynamic roughness.

For the two remaining sites, Tundra and Taiga, no concluding results were obtained. Although the results of this study for the GSL and Wetland sites are encouraging, one should be cautious, however, because there is a need for additional investigation of this procedure.

8. References

Arya, S.P. (2001). Introduction to micrometeorology. Academic Press, p. 420.

Bigg, G.R. (1996). The oceans and climate. Cambridge University Press, 278 p.

Berkowice, R., Prahm, L.P. (1982). Sensible heat flux estimated from routine meteorological data by resistance method. *Journal of Applied Meteorology and Climatology*, Vol. 21, no 12, p. 1845-1864.

Bertoldi, G., Kustas, W.P., Albertson, J.D. (2008). Estimating spatial variability in atmospheric properties over remotely sensed land surface conditions. *Journal of Applied Meteorology and Climatology*, Vol. 47, no 8, p. 2147-2165.

Bolle, H.J. (1997). Remote sensing and radiometric properties of the surface: assessment of desertification from space. Final Report, Contract no: EV5V-CT93-0284, EFEDA Phase II, Group V, p. 208.

Brutsart, W. (2005). Hydrology, an introduction. Cambridge University Press, 605 p.

Burba, G.G., Verma, S.B., Kim, J. (1999). Energy fluxes of an open water area in a mid-latitude prairie wetland. *Boundary-Layer Meteorology*, Vol. 91, p. 495-504.

Businger, J.A. (1988). A note on the Businger-Dyer profiles. *Boundary-Layer Meteorology*, Vol. 42, p. 145-151.

Businger, J.A., Wyngaard, J.C., Izumi. Y., Bradley, E.F. (1971). Flux-profile relationships in the atmospheric surface layer, *Journal of the Atmospheric Sciences*, Vol. 28, no 2, p. 181-189.

Cao, Z., Ma, J., Rouse, W. (2006). Improving computation of sensible heat flux over a water surface using the variation method. *Journal of Hydrometeorology*, Vol. 7, no 4, p. 678-686.

Castellvi, F., Coba, M., Coveta, O.P. (2006). Estimating sensible and latent heat fluxes over rice using surface renewal. *Agricultural and Forest Meteorology*, Vol. 139, no 1-2, p. 164-169.

Dejong, J.M., DeVries, A.C., Klaasen, W. (1999). Influence of obstacles on the aerodynamic roughness of the Netherlands. *Boundary-Layer Meteorology*, Vol. 91, p. 51-64.

Dutton, J.A., Bryson, R.A. (1962). Heat flux in Lake Mendota. *Limnology and Oceanography*, Vol. 7, no 1, p. 80-97.

Fily, M., Royer, A., Goïta, K., Prigent, C. (2003). A simple retrieval method for land surface temperature and fraction of water surface determination from satellite microwave brightness temperatures in sub-arctic areas. *Remote Sens. of Environment*, Vol. 85, p. 328-338.

Garratt, J.R. (1992). The atmospheric boundary layer. Cambridge University Press, p.336.

Garratt, J.R., Hicks, R.B.B. (1973). Momentum heat and water vapour transfer to and from natural and artificial surfaces. *Quarterly Journal of the Royal Meteorological Society*, Vol. 104, p. 491-502.

Hogstorm, U. (1985). Von Karman's constant in atmospheric boundary layer now revaluated. *Journal of the Atmospheric Sciences*. Vol. 42, p. 263-270.

Holton, R.J. (2004). An introduction to dynamic meteorology. Academic Press, p. 535.

Humes, K.S., Kustas, W.P. Goodrich .D.C. (1997). Spatially distribution sensible heat flux over a semiarid watershed. Part I: Use of radiometric surface temperatures and spatially uniform resistance. *Journal of Applied Meteorology*, Vol. 34, no 4, p. 281-292.

Jia, L. (2004). Modelling heat exchanges at the land atmosphere interface using multi-angular thermal infrared measurements. Ph.D. thesis, Wageningen University, 199 p.

Jiang, L., Islam, S., Carlson, T.N. (2004). Uncertainties in latent heat flux measurement and estimation, implications for using a simplified approach with remote sensing data. *Canadian Journal of Remote Sensing*, Vol. 30, no 5, p. 769-787.

Kodama, Y., Sato, N., Yabuki, H., Ishii, Y., Nomura, M., Ohata, T. (2007). Wind direction dependency of water and energy fluxes and synoptic conditions over a tundra near Tiksi, Siberia. *Hydrological Processes*, Vol. 21, no 15, p. 2028-2037.

Kampf, S.K., Tyler, S.W. (2006). Evaporation and land surface energy budget at the Salar de Atacama, Northern Chile. *Advances in Water Resources*, Vol. 29, p. 336-345.

Kustas, W.P., Stannard, D.I., Allwine, K.J. (1996). Variability in surface energy flux partitioning during Washita'92: resulting effects on Penman-Monteith and Priestley-Taylor parameters. *Agricultural and Forest Meteorology*. Vol. 82, p. 171-193.

Köhn, J. (2006). Caractérisation de la température de la neige par télédétection micro-onde passive au Canada. Thèse de maîtrise, Département de géomatique appliquée, Université de Sherbrooke, 86 p.

Lackmann, G.M., Gyakum. J.R. (1996). The synoptic- and planetary-scale signatures of precipitating systems over the Mackenzie River Basin. *Atmosphere-Ocean*, Vol. 34, no 4, p. 647-674.

Latifovic, R., Zhu, Z., Cihlar, J., Giri, C. (2002). Land cover of North America 2002. Natural Resources Canada, Canada Centre for Remote Sensing, US Geological Survey EROS Data Center.

Leon, L.F., Lam., Schertzer, D.W., Swayne D. (2005). Lake and climate models linkage: a 3-D hydrodynamic contribution. *Advances in Geosciences*, Vol. 4, p. 57-62.

Long, Z., W. Perrie, J. Gyakum, R. Laprise., Caya, D. (2007). Northern lake impacts on local seasonal climate. *Journal of Hydrometeorology*, Vol. 8, no 4, p. 881-896.

Ma, Y., Ishikawa, H. (2003). Regionalization of surface fluxes over heterogeneous landscape of the Tibetan Plateau by using satellite remote sensing data. *Journal of the Meteorological Society of Japan*, Vol. 81, no 2, p. 277-293.

Manlio. B. (1989). Inconsistent surface flux partitioning by the Bowen ratio method. *Boundary-Layer Meteorology*. Vol. 49, no 1-2, p.149-167.

Mesinger, F. Co-authors (2006) North American Regional Reanalysis, *Bull. Of Amer.Meteor. Soc*, Vol 87, Iss 3, p. 343-360

Mialon, A., Royer, A., Fily, M., Picard, G. (2007). Daily Microwave-Derived Surface Temperature over Canada/Alaska. *Journal of applied meteorology and climatology*, Vol. 46, p. 591-604

Mialon, A. (2005). Étude de la variabilité climatique des hautes latitudes nord, dérivée d'observations satellites micro-ondes. Thèse de doctorat, Département de géomatique appliquée, Université de Sherbrooke – LGGE, Université de Grenoble, 235 p.

Monteith, J.L. (1973). Principles of environmental physics. Elsevier, 241 p.

Momii, K., Ito Y. (2008). Heat budget estimates for Lake Ikeda, Japan *Journal of Hydrology*, Vol. 361. p. 362-370.

Nagarajan, B., Yau, M.K., Schuepp, P.H. (2004). The effects of small water bodies on the atmospheric heat and water budgets over the Mackenzie River Basin. *Hydrological Processes*. Vol. 18, p. 913-938.

Pan, J., Yan, X.H., Jo. Y.H., Zheng Q., Lio, W.T. (2003). A new method for estimation of the sensible heat flux under unstable conditions using satellite vector winds. *Journal of Physical Oceanography*, Vol. 34, p. 968-977.

Panin, G., Nasonov, A., Foken, Th., Lohse, H. (2006). On the parameterization of evaporation and sensible heat exchange for shallow lakes. *Theoretical and Applied Climatology*, Vol. 85, p. 123-129.

Quattrochi, D., Luvall, L. (2004). Thermal remote sensing in land surface processes. CRC Press, 440 p.

Revfeim, K.J.A., Jordan, R.B. (1976). Precision of evaporation measurement using the Bowen ratio. *Boundary-Layer Meteorology*, Vol. 10, no. 2, p. 97-111.

Rouse, W., R., Schertzer, D. W., William, M. (2005). The role of Northern Lakes in a regional energy balance. *Journal of Hydrometeorology*, Vol. 6, no 3, p. 291-305.

Rouse, W., Eaton, A., Lafleur, M., Marsh, P. (2001). Surface energy balance of the western and central Canadian subarctic. *Journal of Climate*, Vol. 14, p. 3692-3703.

Rouse, W., Spence, C. (2003). The energy budget of a small Canadian Shield lake. *Journal of Hydrometeorology*, Vol. 4, p. 649-701.

Sato, N. (2004). Water transport process of air -vegetation-soil system in the arctic tundra. Ph.D. thesis, Graduate School of Environmental Earth Science, Hokkaido University, Sapporo, Japan, 86 p.

Schindler, D.W. (2001). The cumulative effects of climate warming and other human stresses on Canadian freshwaters in the new millennium. *Canadian Journal of Fisheries and Aquatic Sciences*, Vol. 58, p. 18-29.

Segal, M., Arritt, R.W. (1992). Nonclassical mesoscale circulation caused by surface sensible heat flux gradients. *Bulletin of the American Meteorological Society,* Vol. 73, no 10, p. 1593-1622.

Spence, C., W. R. Rouse. (2002). The energy budget of subarctic Canadian Shield terrain and its impact on hillslope hydrology. *J. Hydrometeorology,* Vol. 3, no 2, p 208–218

Stull, R.B. (1988). An introduction to boundary layer meteorology. Kluwer Academic, 679 p.

Stull, R.B. (2000). Meteorology for scientists and engineers. Brooks Cole, 502 p.

Sugita, M., Brutseart, W. (1990). Regional surface fluxes from remotely sensed skin temperature and lower boundary-layer measurements. *Water Resources Research*, Vol. 26, p. 2937-2944.

Sun, J., Esbensen, S.K., Mahrt, L. (1995). Estimation of surface heat flux. *Journal of the Atmospheric Sciences*, Vol. 52, no 7, p. 3162-3171.

Swayne, D., Lam, D., Mackay, M., Rouse, W., Schertzer, W. (2005). Assessment of the interaction between the Canadian Regional Climate Model and lake thermal-hydrodynamic models. *Environmental Modeling & Software*, Vol. 20, p. 1505-1513.

Swayne, D., Sharma, V., Lamb, D., MacKay, M., Rouse, W., Schertze, W., Hunga, P. (2004). A spatially parallel implementation of a lake and land surface model interaction with a regional climate model, http:// www.iemss.org/iemss2004/pdf/Kyoto/ swayaspa.pdf.

Tanner, B.D., Greene, J.P., Bingham, G.E. (1987). A Bowen-ratio design for long term measurements. ASAE Paper no 87-2503, American Society of Agricultural Engineers. St. Joseph, MI, 1-6.

Thom, A.S. (1972). Momentum, mass and heat exchange of vegetation. *Quarterly Journal of the Royal Meteorological Society*, Vol. 98, p. 124-134.

Webb, E.K. (1970). Profile relationships: The log-linear range and extension to strong stability. *Quarterly Journal of the Royal Meteorological Society*, Vol. 112, p. 857-889.

Appendix 1

Table A. 1- Classification of land covers

1	Tropical or sub-tropical broadleaved Evergreen Forest - closed canopy
2	Tropical or sub-tropical broadleaved Decidous Forest - closed canopy
3	Temperate or sub-polar broadleaved Decidous Forest - closed canopy
4	Temperate or sub-polar Needleleaved Evergreen Forest - closed canopy
5	Temperate or sub-polar Needleleaved Evergreen Forest - open canopy
6	Temperate or sub-polar Needleleaved mixed Forest - closed canopy
7	Temperate or sub-polar Mixed broadleaved or Needleleaved Forest - closed canopy
8	Temperate or sub-polar Mixed broadleaved or Needleleaved Forest - open canopy
9	Temperate or sub-polar Broadleaved Evergreen Shrubland - closed canopy
10	Temperate or sub-polar Broadleaved-Decidous Shrubland - open canopy
11	Temperate or sub-polar Needleleaved-Evergreen Shrubland - open canopy
12	Temperate or sub-polar Mixed Broadleaved or Needleleaved-Dwarf-Shrubland - open canopy
13	Temperate or sub-polar grassland
14	Temperate or sub-polar grassland with a sparse tree layer
15	Temperate or sub-polar grassland with a sparse shrub layer
16	Polar grassland with a sparse shrub layer
17	Polar grassland with a dwarf-sparse shrub layer
18	Cropland
19	Cropland and Shrubland/woodland
20	Subpolar Needleleaved Evergreen Forest Open Canopy - lichen understory
21	Unconsolidated Material Sparse vegetation (old burnt or other disturbance)
22	urban or built up
23	consolidated Rock sparse vegetation
24	waterbodies
25	resent burnt area
26	snow and ice
27	wetlands
28	herbaceous wetlands
29	ocean

Appendix 2

Table A. 2- Value of aerodynamic roughness length and canopy height derived from Garrate 1992, Pielke 2002 and Eco-forestry map

Surface	Z(m)	h_c
Water bodies	0.0002 (Pielke 2002)	0
Sparse Vegetation	0.002 (Deacon 1953)	0.025
Crops	0.025 (Izumi 1971)	0.25
Grass land	0.2 (Fichtl and McVehil (1970)	1.0
Trees	0.4 (Garratt 1980)	8.0
Forest	0.55 0.92 (Thom et al. 1975)	13.3 15.8

Appendix 3

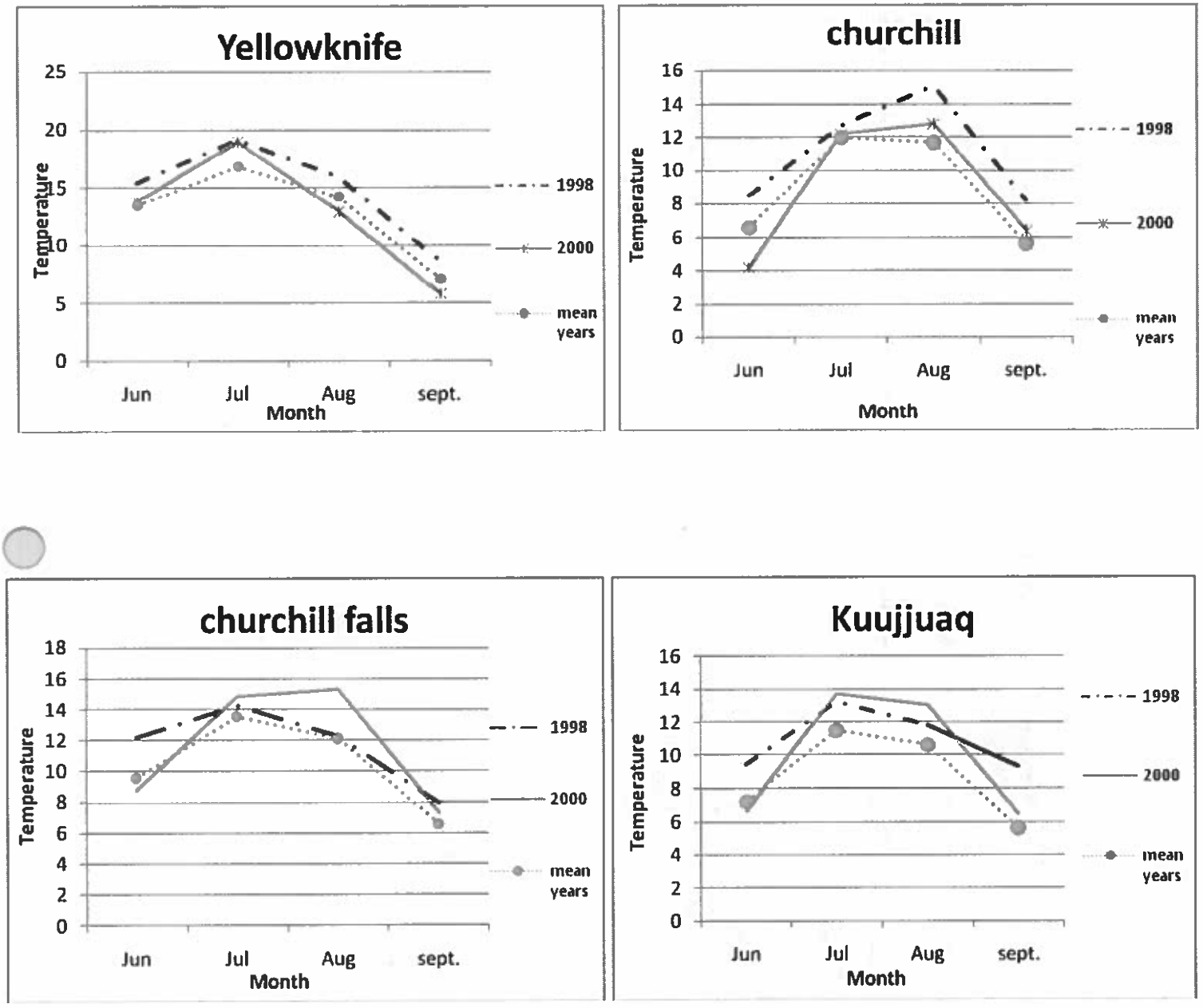

Figure A. 2- Temperature condition over two summers, 1998 and 2000 (comparison with 30 years 1970-2000)

Appendix 4

Table A. 3- The retrieved values for GSL site

Class	Small FWS (SF)				Medium FWS (MF)				Large FWS(LF)			
Period	Early		Late		Early		Late		Early		Late	
year	1998	2000	1998	2000	1998	2000	1998	2000	1998	2000	1998	2000
y	-8.35	-3.19	-19.45	-25.44	-3.89	-1.26	-12.27	-12.87	0.58	4.13	-2.34	-5.15
x	-23.71	-28.76	-37.70	-49.22	-23.71	-28.76	-37.70	-49.22	-23.71	-28.76	-37.70	-49.22
R	+0.35	+0.11	+0.51	+0.51	+0.16	+0.04	+0.32	+0.26	-0.02	-0.14	+0.06	+0.10

Table A.4- The modelled devalues for GSL site

Class	Small FWS (SF)				Medium FWS (MF)				Large FWS(LF)			
Period	Early		Late		Early		Late		Early		Late	
year	1998	2000	1998	2000	1998	2000	1998	2000	1998	2000	1998	2000
y	-57.83	-69.36	-29.74	-54.99	-54.94	-63.27	-29.34	-51.38	-9.35	-06.76	-06.98	-13.10
x	-67.89	-77.55	-39.66	-58.85	-67.89	-77.55	-39.66	-58.85	-67.89	-77.55	-39.66	-58.85
R	+ 0.85	+0.89	+0.75	+0.93	+0.80	+0.81	+0.74	+0.87	+0.13	+0.08	+0.17	+0.22'